Materials
Advances

ROYAL SOCIETY
OF **CHEMISTRY**

PERSPECTIVE
Rodolphe Antoine *et al.*
The emergence of mass spectrometry for characterizing
nanomaterials. Atomically precise nanoclusters and beyond

Check for updates

The emergence of mass spectrometry for characterizing nanomaterials. Atomically precise nanoclusters and beyond

Clothilde Comby-Zerbino, Xavier Dagany, Fabien Chirot, [ID] Philippe Dugourd [ID] and Rodolphe Antoine [ID] *

Mass spectrometry (MS) is widely used in molecular science, and is now emerging as a characterization technique for ultra-small nanoparticles. In the field of atomically precise nanoclusters, MS combined to ionization sources such as electrospray and matrix-assisted laser desorption-ionization allows for accurate characterization of the size and charge state of the metal core and of the number of ligands. MS also enables monitoring the evolution of these characteristics during synthesis. When dispersion in nanomaterial composition increases, more relevant metrics are average mass and mass distribution, which can be estimated from electrospray mass spectra using correlation algorithms. Also complex mixtures can be analysed using separation techniques directly coupled with mass spectrometry. For larger nanomaterial compounds, cutting-edge charge detection mass spectrometry can even be used to access the megadalton mass range. In addition, recent MS advancements include the development of new hyphenated techniques such as ion mobility and action spectroscopy, revealing structural details and structure-optical properties relationships in these systems. The present perspective aims at capturing the growing importance and impact of these mass spectrometry based techniques completing the characterization toolbox in materials science.

1 Introduction

A century ago, the first mass spectrometer – originally called a parabola spectrograph – was constructed by Sir J.J. Thomson and gave birth to mass spectrometry (MS) by measuring the mass-to-charge ratio (m/z) values of gaseous ionized molecules.[1] Then, mass spectrometry has been strongly associated with the analysis of organic molecules for which ionization techniques like electric discharge and electron impact were optimal.[2] Slowly, the field of mass spectrometry moved towards more complex molecules like sugars, DNAs, and peptides but was hampered by the lack of efficient, non-destructive ionization methods. In late 1980's, the development of electrospray ionization (ESI)[3] and of laser desorption based methods[4] like matrix-assisted laser desorption ionization (MALDI)[5] pushed the limit for ionization of macromolecules and constituted a breakthrough in MS, in particular for protein analysis.[6] In parallel, mass spectrometers became more and more sensitive and accurate, with high resolving power. For instance sub ppb sensitivity and sub-ppm mass accuracy are now routinely available (at moderate cost) from benchtop

MS instruments.[7,8] Beyond unique capabilities for the determination of chemical composition, MS can also provide structural information at different levels. It can be coupled to numerous dissociation techniques,[9–11] thus enabling characterization of molecular bonding networks. Molecular species can also be characterized in terms of 3-dimensional structure and structural dispersity, based on the coupling of mass spectrometry with ion mobility spectrometry.[12]

The capabilities of MS for composition and structure determination can be applied to the investigation of nanostructured materials.[13] In particular, ultrasmall nanoparticles (USNPs), with sizes in the 1–3 nm range, exhibit unique properties, distinct from those of free molecules and larger-sized nanoparticles. However, the plethora of well-established analytical techniques used for obtaining the size distribution of nanoparticles (NPs) and information on their structure (*e.g.* transmission electron microscopy (TEM), scanning electron microscopy (SEM), dynamic light scattering (DLS), atomic force microscopy) are often not accurate enough to address size and associated dispersion for USNPs.[14] In contrast, the typical molecular weights of USNPs is easily accessible with current mass spectrometers: USNPs lay in the kilo-Dalton (kDa) to mega-Dalton (MDa) mass range (Dalton, abbreviated Da, is a unit used in expressing atomic or molecular mass, defined as 1/12 the mass of a single

Univ Lyon, Université Claude Bernard Lyon 1, CNRS, Institut Lumière Matière, UMR 5306, F-69622 Lyon, France. E-mail: rodolphe.antoine@univ-lyon1.fr

atom of carbon-12). Moreover, soft ionization sources (ESI or MALDI) have proven to be extremely versatile to ionize and transfer intact USNPs in the gas phase.[15–18]

The properties of USNPs are greatly sensitive to both their composition and size. Developing strategies for producing USNPs with atomic precision, *e.g.* ultrasmall nanoparticles produced with a unique number of atoms (often called atomically precise nanoclusters) remains the holy grail in the field.[19,20] In terms of structure, such atomically precise nanoclusters can be viewed as a "multi-shell system" composed of a metallic core, a metal–ligand interface, and the surface ligand molecules. Mass spectrometry is facing several challenges such as characterizing both the core size and its charge state, the number of protecting ligands, thus yielding a stoichiometry between ligand and metal. Current synthesis often involves complex ligand engineering strategies. The ligands themselves can be complex, for example large proteins, or large synthetic polymers can be employed as templates. On the other hand, multi-shells of different ligands also offer interesting possibilities, but in turn, adding mass dispersion when atomic precision is not reached. Thus, the characterization of such engineered USNPs by mass spectrometry has to find the right balance between the precise determination of metal/ligand stoichiometry and a proper characterization of mass dispersity. This review, illustrated by pedagogic examples from the literature, aims at providing an overview of the recent advances in the characterization of protected metal nanoclusters by mass spectrometry. We will particularly focus on the different challenges related to the different levels of mass dispersity displayed by UNSPs ranging in the kilodalton to the megadalton mass range.

2 Mass spectrometry of nanomaterials

In the 1980s, thanks to the development of advanced cluster sources (supersonic expansion, laser-desorption ionization sources),[21,22] mass spectrometry became an indispensable tool for the characterization of gas-phase bare metal clusters,[23,24] as well as fullerenes,[25] carbon[26] and silicon clusters.[27,28] In the 1990s, the landmark synthesis by Brust and co-workers of thiolate monolayer-protected gold nanoparticles, opened the route to reach gold core dimensions smaller than 3 nm by wet chemistry synthesis.[29,30] These ultra-small nanoparticles (often called monolayer-protected clusters) have been representing an active field in nanoscale community these last 15 years. Following the Brust synthesis, Whetten and co-workers did seminal works to determining the chemical composition of gold nanoclusters in the 1–3 nm size range, using mass spectrometry (in the 10–300 kDa mass range).[31–34] Since then, MS has been growingly used by material chemists and inorganic chemists for the characterization of various types of ultra-small nanoparticles and nanoclusters. Most MS analyses conducted on nanoclusters were done using either ESI or MALDI ionization sources in both positive and negative modes.[17,35] ESI is known to produce gas-phase ions with relatively broad charge states distributions. In contrast, MALDI (due to the inherent low charge transfer process between matrix and analytes) generally yields ions with lower charge states (typically 1 or 2 charges per ion), resulting in narrower charge distributions, as illustrated by Fig. 1 (left bottom panel). In the following, we will mainly focus on reviewing MS examples on monolayer-protected metal clusters. Atomically precise nanoclusters (NCs) are designed to contain a definite number of core metal atoms, protected by a well-defined number of surface ligands. Consequently, the mass spectra
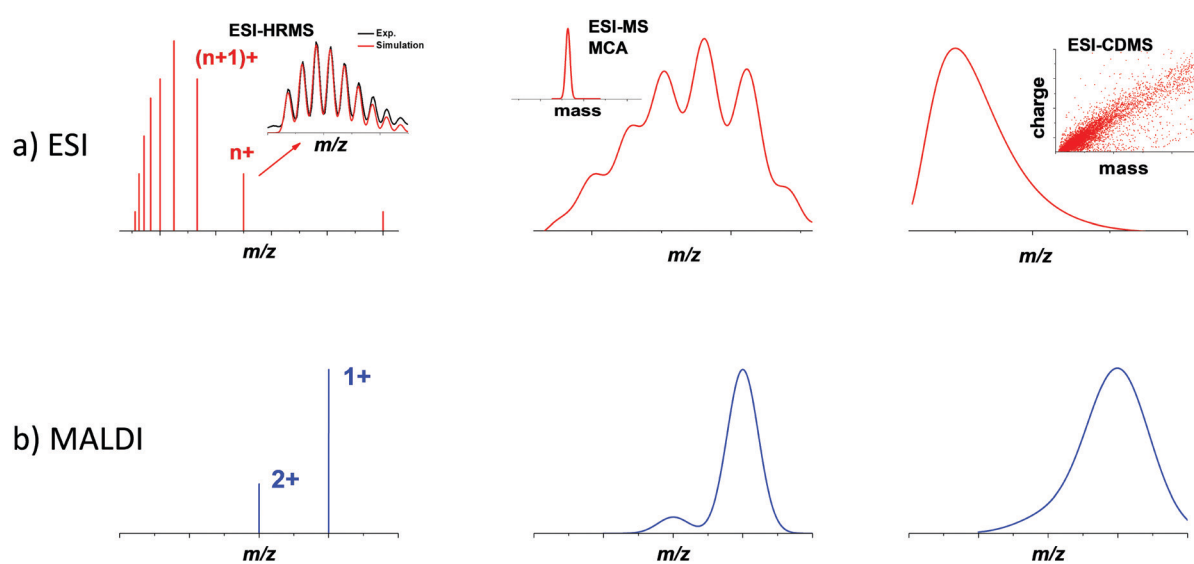

Fig. 1 Schematic illustration of mass spectra with ESI and MALDI ionization sources and mass spectrometry devices for nanomaterials with increasing mass and dispersity. High-resolution mass spectrometry (HRMS) is usually used for atomically precise nanoclusters, multiplicative correlation algorithm (MCA) in combination with ESI-MS may be useful for mass characterization of polydisperse nanoclusters (in the mass range 10–100 kDa), while for nanomaterials with mass exceeding megadalton, mass distribution can be obtained using charge detection mass spectrometry (CDMS).

obtained for such nanoclusters show similarities with that of large molecules. They usually display sharp peaks corresponding to species with the exact same composition in terms of the number of core atoms and surface ligands. Depending on the ionization source, species with different net charges are often present, yielding a series of peaks (see Fig. 1 left panel). If such simple and clean spectra are acquired with sufficient mass resolution and accuracy, it is often possible to resolve an isotopic pattern and to precisely determine the monoisotopic mass of the nano-clusters. As for molecular species, assignment of an atomic composition is then possible, based on a match between the measured value of the monoisotopic mass and that computed for candidate raw formulas. Such assignment can even be consolidated by the comparison of the experimental isotope pattern (relative intensity of the different peaks) to simulated isotopic distributions. In this vein, careful studies using high resolution mass spectrometry (HRMS) from Murray[36–38] and coworkers and Tsukuda and coworkers,[39–44] among others, have determined the molecular formulas (*e.g.* number of metal atoms and number of ligands) of metal nanoclusters. Long confined to a technique among many others, MS and in particular HRMS is currently emerging as a gold standard for characterizing atomically precise nanoclusters.[16,17] Further applications of HRMS will be described in Section 2.1.

Atomic precision is nevertheless rarely fully achieved, and nanocluster samples often display some dispersity in their composition. Dispersity can arise from the number of protecting ligands, even if the number of core atoms is conserved among the different species. When several ligands are present, different stoichiometry can also be observed. Moreover, oligomers corres-ponding to the bonding between different clusters, with or without coalescence of the cores, is also possible, as well as partial degradation of the species initially synthesized. All these sources of dispersity yield species with different masses, which can, in principle, be separated and characterized by mass spectrometry. Additionally, structural dispersity (*i.e.* the coexistence of different isomers), or charge dispersity (different charge states, especially of the core) are also important to characterize. However, their impact on the mass and charge distributions observed by MS is often difficult to interpret, and requires complementary methods (see Section 3).

Even if a plethora of peaks are observed in mass spectra, it is in principle possible, using high resolution and high precision instruments to assign a raw formula to each peak. However, the instruments required are extremely expensive, and the deconvolution procedures are relatively complicated and time-consuming. Moreover, the combination of the above-cited dispersity factors often lead to "quasi-continuous" mass distributions (see Fig. 1 middle panel), with large dynamic range in concentrations, which makes any mass assignment often impossible. In such cases anyway, the exhaustive determination of all species present, is not only unattainable, but also poorly relevant. However, determining the average mass in a polydisperse cluster sample is of paramount interest, because it allows estimating the average core size and the average number of ligands. Based on advanced deconvolution
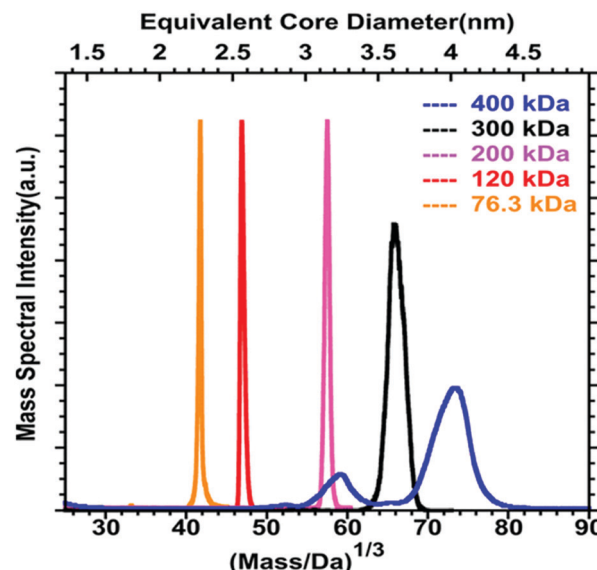

Fig. 2 MALDI-MS of 76.3 to 400 kDa nanoparticles synthesized using HSC$_6$H$_{13}$ thiol. Mass spectrum data are plotted *versus* the cube root of mass to allow comparison with the core equivalent diameter (reprinted with permission Copyright© 2018 American Chemistry Society).[45]

procedures for ESI-MS spectra and using assumptions for average charge states for MALDI-MS spectra, it is possible to extract an average mass and its dispersion for small polydisperse nanoparticles. For instance, Dass and coworkers pushed the limit of MALDI-MS analysis for mass characterization of large gold NCs, in the sub-megadalton range of mass, as displayed in Fig. 2. But here, some assumptions on the charge state and on the power correlation between the number of gold atoms and the thiolate ligands are required to obtain a chemical composition.[45,46] The potential of MS to determine the average composition of polydisperse clusters in terms of ligands and core size, and the associated dispersion (instead of raw formulas) will be discussed in Section 2.2.

Finally, when nanoparticles are produced without atomic precision, then size and mass dispersions can be high and when masses exceed several megadaltons, mass spectra are characterized by a broad envelope without any resolved pattern (see Fig. 1 right panel). Without hypothesis on the average charge of nanoparticles, it is impossible to extract information from mass spectra. We will show however that charge detection mass spectrometry that measures the mass (or more exactly *m*/*z*) and charge at the single ion level can provide accurate mass distributions for larger nanoparticles (see Section 2.3).

2.1 High-resolution mass spectrometry for atomically precise nanoclusters

Modern mass spectrometers, in particular based on the time-of-flight technology widely used in the nanoclusters community, can reach high resolving power ($>50\,000$) and mass accuracy ($\leq$few ppm). With such mass accuracy and resolution capabilities, then the comparison between experimental and simulated isotopic distribution pattern (of the Au, Ag, Pt, Pd, *etc.* metals and that of
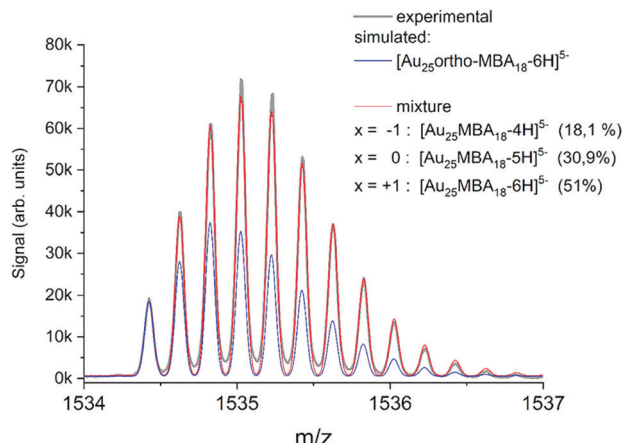
Fig. 3 (Black line) Experimental isotope pattern for $[Au_{25}\text{-}ortho\text{-}MBA_{18}]^{5-}$. (Blue line) Simulated isotope patters for $[Au_{25}\text{-}ortho\text{-}MBA_{18}\text{-}6H]^{5-}$ adjusted to fit the intensity of the experimental monoisotopic peak. (Red line) Fit obtained by considering a mixture of species with different deprotonation patterns, corresponding to different charge shifts x. (reprinted with permission Copyright© 2020 American Chemistry Society).[47]

atoms present in the ligands) for a given chemical formula (M_nL_m: n number of M metal and m number of L ligand) allow for "confident" nanocluster assignment. As an illustration, ESI-HRMS of Au_{25} protected by 18 MBA ligands (MBA mercaptobenzoic acid) is presented in Fig. 3. Of note, the observed isotope pattern was resulting from the coexistence of species with different raw formulas, including $[Au_{25}\text{-}ortho\text{-}MBA_{18}\text{-}6H]^{5-}$ but also $[Au_{25}\text{-}ortho\text{-}MBA_{18}\text{-}5H]^{5-}$ and $[Au_{25}\text{-}ortho\text{-}MBA_{18}\text{-}4H]^{5-}$ in respective proportions of 51.0%, 30.9%, and 18.1%.[47] Clearly, as pointed out by Hayton and coworkers,[48] the comparison of simulated isotope patterns and masses of observed mass spectral peaks should be taken with great care, since many factors can affect mass spectra (ion suppression, ion fragmentation, and adduct formations and reactions with the matrix...). Indeed, many works in the literature using MS as "characterization tool" have led to erroneous mass assignment of nanoclusters. One of the most striking examples was given by new chemical compositions of the glutathione protected gold clusters determined previously by electrospray ionization (ESI) mass spectrometry and reassessed by taking advantage of freshly prepared samples, higher mass resolution, and more accurate mass calibration.[41] It also worth citing the story of monodisperse $Au_{25}L_{18}$, initially identified as $Au_{28}L_{16}$ and as $Au_{38}L_{24}$ before a correctly identification could be done by electrospray-ionization mass spectrometry.[49] Even with MS instrument providing high resolution and high mass accuracy, gas phase NCs may appear in the form of $[M_nL_m \pm xH]^{z+/-}$ (addition of protons or deprotonations) or $[M_nL_m + xAd]^{z+}$, $[M_nL_m + yAd]^{z-}$ (addition of other adduct ions, Ad, present in synthetic process). Such adducts may induce difficulties or even errors to correctly assign the nanocluster composition.[50] For mixtures of nanoclusters, performing desalting procedure before MS analysis, can lead to much better mass assignment.[51] Usually, the composition, size, and monodispersity can be determined by high resolution mass spectrometry for atomically precise nanoclusters, in addition with other characterization techniques (usually NMR, FT-IR,

X-ray absorption and photoelectron spectroscopies), and this was done mostly for nanoclusters containing gold or silver.[52–79] HRMS was also applied for characterizing atomically monodisperse copper,[80–86] nickel,[87–89] cobalt,[90] palladium[91] nanoclusters and molecule-like CdSe nanoclusters.[92]

In order to better tune chemical/physical properties of atomically precise metal nanoclusters, several strategies have been adopted in particular using either ligand engineering or metallic kernel (or core) alloying. Synthesis and composition characterization of alloyed nanoclusters are necessary from both scientific and practical aspects.[93] Due to specific isotope patterns of the metals (Au, Ag, Pt, Pd, *etc.*), HR-MS has proven particularly useful to determine the composition of alloyed nanoclusters, in particular for gold-doped silver[94–98] and silver-doped gold[99–103] nanoclusters. MS investigations of Pt and Pd doping on noble metal clusters were also reported.[104–108] High-resolution mass spectrometry was also applied to monitor the atom-by-atom substitution of Fe and Ni to the core of a well-defined ligated cobalt nanocluster.[109] Alloying metallic kernel from monometallic to tetrametallic was also demonstrated and the monodispersity of each alloyed nanocluster was characterized by electrospray ionization mass spectrometry analysis.[98,110] By recording mass spectra as a function of time, the evolution of the composition of a reacting mixture can even be monitored, which allows a better comprehension of the formation process, especially for alloyed nanoclusters.[108,111–114] The Xie group and Pradeep group did impressive works using these approaches.[16,17] In particular, time-dependent electrospray ionization mass spectrometry was found to be a powerful tool to follow the formation of $MAu_x Ag_{28-x}(BDT)_{12}(PPh_3)_4$ ($x = 1$–12) and bimetallic $Ag_xAu_{25-x}(PET)_{18}$ ($x = 1$–7) NCs during complex intercluster reaction, as illustrated in Fig. 4.[110,115]

Surface modification by specific functional groups is another effective approach to tune properties of nanoclusters for practical applications. Current strategies to engineer surface of metal nanoclusters employ multiple protecting ligands, ligand exchange or etching processes. Murray and co-workers studied Au_{25} NCs with ligand-exchanged mixed monolayers (thiophenolate, hexanethiolate, or biotinylated ligands) using ESI-MS.[116,117] Mass spectrometry was again powerful for characterizing ligand exchange reactions in protected nanoclusters with selenolates or tellurolates.[118–121] Again, time dependent experiments have permitted to push forward the understanding of the formation of cluster size conversion or surface ligand modifications as a function of ligand exchange strategies,[122–126] reactive agents[127–133] or etching process.[134,135]

Probing the charge state of the metal core (or kernel) of nanoclusters is also an exciting field of investigation. Indeed the total charge on nanoclusters may drive its reactivity.[122,136,137] Therefore, efficient tools able to probe the charge states of metal nanoclusters are critical to investigate their potential application. Nuclear magnetic resonance (NMR), cyclic voltammetry[138] and optical absorption spectroscopy can be used to address the charge state of metal nanoclusters.[139–141] However, MS approaches were also successful. On the basis of
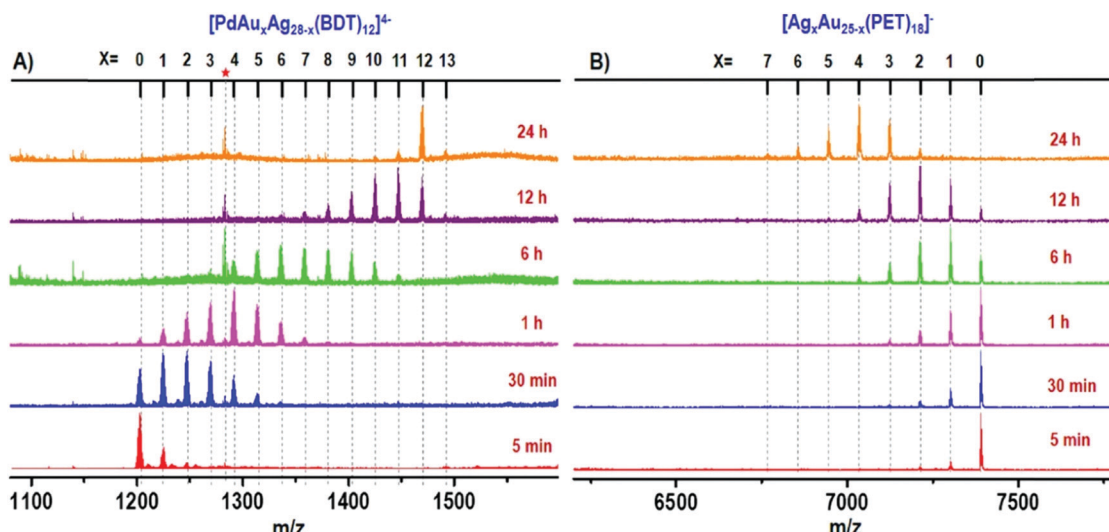
Fig. 4 Time-dependent ESI MS of intercluster reaction between $PdAg_{28}$ and Au_{25} (1:5 ratio) where panel (A) shows the reaction at the $PdAg_{28}$ side and panel (B) presents the reaction at the Au_{25} side. The red asterisk corresponds to thiolates produced during the reaction. The species observed are $[PdAu_xAg_{28-x}(BDT)_{12}]^{4-}$ and $[Ag_xAu_{25-x}(PET)_{18}]^{-}$. (reprinted with permission Copyright© 2019 American Chemistry Society).[110]

detailed ESI-MS analysis, Tsukuda and coworkers studied the charge states of Au_{25} nanoclusters.[142] Following this approach, our group further investigated Au NCs protected by glutathione ligands.[143] The charge assignment was complicated by the fact that the total charge of the cluster ($[Au_n(SG)_m\text{-}(p)H]^{q-}$) is a combination of p charges hold by several deprotonations on ligands and the charge of the gold kernel (q-p). In particular, using glutathione as ligand molecule, clusters with sizes superior to $Au_{22}(SG)_{17}$ were found to bear a negative kernel charge. Indeed, for such sizes, the gold core is sufficiently large to accommodate an excess electron. Charge states for clusters protected by "neutral" ligands (that do not ionize easily in the gas phase) were also reported in the literature using extra charging with alkali adducts[144] or in the negative mode of ionization of electrospray for nanoclusters holding negative charges on the cluster core.[145] Finally, our group has recently investigated the heterogeneity in the charging patterns of $Au_{25}MBA_{18}$ clusters by mass spectrometry. For a given charge state of those clusters, it was shown that several populations with different protonation patterns coexist (see Fig. 3).[47]

2.2 Mass spectrometry for polydisperse nanoclusters. Multiplicative correlation algorithm

Atomically precise nanoclusters are only a narrow class of ultra-small nanoparticles. Generally, synthesis lead to mixtures of clusters composed of different numbers of both core atoms and of the surface capping agents leads to charge and mass dispersion. This is particularly true for a specific class of nanocluster, e.g. protein templated metal nanoclusters. While ESI-MS is the gold standard for analyzing many proteins, only very few analyses of protein protected clusters by ESI MS have been reported.[146] It is likely that ESI ionization efficiency is dramatically lowered due to the presence of counter ions from the synthesis procedure.[147] Following the first MALDI-MS spectrum reported by Xie and coworkers for BSA-templated gold

nanoclusters,[148] efforts have been made, mainly by Pradeep's group, to use MALDI-MS to characterize protein-templated metal nanoclusters.[149] MALDI matrices are crystal-forming organic molecules used to enhance the vaporization of poorly-volatile analytes, and their ionization through charge transfer capability. Typically sinapic acid (SA), α-cyano-α-hydroxy cinnamic acid (CHCA) and others,[150] used for proteins are also suitable for protein-templated metal nanoclusters. Commercial MALDI TOF instruments coupled to standard 337 nm N_2 laser are generally used. MALDI-MS spectra usually show both bare proteins and the corresponding protein-templated metal nanoclusters displaying a broad unresolved peak shifted by few kDa due to the presence of the gold core. However, the observed broad envelopes on MS spectra prevent from any clear assignment of the exact number of gold atoms and its possible dispersion. So far, gold and silver nanoclusters templated by a large variety of proteins (i.e. bovine and human serum albumin, bovine lactoferrin, human serum transferrin, hemoglobin, insulin, lysozyme, trypsin, horse radish peroxidase, pepsin, egg white, egg shell membrane, human hair, chymotrypsin) have been characterized by MALDI-MS, as reviewed by Pradeep et al.[53,149]

Beyond mass characterization, the mechanisms of the formation of protein-protected nanoclusters have also been investigated by MS. Especially, Pradeep's group used time-dependent mass spectrometry of the reaction mixture in order to systematically monitor the first step of the growth of the cluster within the protein template.[151–153] Matrix-assisted laser desorption ionization mass spectrometry was also used to document the pH-dependent and time-dependent in situ growth of Au NCs in protein.[154] Recently, Shu-Hui Chen and coworkers intended to elucidate the core ligand sequence and key residues responsible for protein-encapsulated gold nanoclusters formation and stabilization using MALDI-MS, LC-MS/MS, and proteomics by developing a proper workflow and sample preparation method.[155]

Other strategies have been explored to tune properties of ultrasmall nanoparticles. For instance, metal clusters can be protected by multi-shells of ligands (using multidentate zwitterionic ligands). Also one can play with the ratio between the reducing and protecting agent leading to a subtle balance between metal kernel and shell of oligomeric Au(I)-ligand complexes. Such strategies in turn yield a strong mass and charge dispersion.[156,157] As an illustration Fig. 5 displays the MALDI-MS spectrum of gold nanoclusters stabilized by a shell of zwitterion ligands (AuZw nanoclusters). A continuous band centered at m/z 14 500 is observed along with equally spaced sharp peaks at lower masses. The broad band corresponds to highly polydisperse intact Au NCs associated with the ligand by covalent and no covalent bonds. Discrete peaks are attributed to the fragmented Au NC core. In such case, the MALDI spectrum clearly contains poor information on the composition of the clusters. Our group proposed to use the ESI ionization mode to better characterize such nanoclusters. Ligands protecting NCs often contain multiple groups easily ionized by ESI. The resulting ions are then highly charged, and different charge states are formed. The ESI spectrum is then more complex than the MALDI spectrum, but still poorly resolved. However, instead of a single broad band corresponding to the whole cluster, a series of bands is visible (as illustrated in Fig. 1 middle panel). These bands correspond to the different charge states of the whole cluster, and their distribution (decreasing inter-distance as m/z decreases) is characteristic of its mass and charge. We developed a multiplicative correlation algorithm (MCA) to estimate the mass of nanoparticles from such spectra.[158,159] The multiplicative correlation was specifically designed to enhance the deconvoluted signal when the parent molecule is distributed into several charge states in the spectrum measured. As seen in Fig. 5, for gold nanoclusters stabilized by a shell of zwitterion ligands, the deconvoluted ESI-MS spectrum allows to determine their mass distribution (centered at 11 000 Da with a second minor distribution at ~13 500 Da).[160] Thus, possible molecular formula for AuZw ($\approx$ 11 kDa) (see Fig. 5c) could be $Au_{12}Zw_{22}$. Such deconvolution approaches with ESI-MS measurements were found to be well-adapted for solving mass distributions of polydisperse gold nanoclusters[51,160–165] as well as for ultrasmall Gd-based silica NPs.[166–173]

2.3 Mass spectrometry beyond nanoclusters. Charge detection mass spectrometry

Larger particles with higher molecular weight, $e.g.$ megadalton or even larger, are also of interest in the nanoscale community. Indeed, recent strategies have emerged to produce self-assemblies of atomically precise noble metal nanoclusters with potential applications in various fields of science. More generally, due to their well-defined structure, metal NCs have become promising functional building blocks of metamaterials for various practical applications. Arrangement of functional building blocks into ordered hierarchy architectures is an alternative means to enhance individual properties by synergetic effects. Such controlled self-assemblies are supposed to have very large molecular weight with strong mass dispersion, beyond the scope of traditional MS techniques. Indeed, for such nanomaterials, the electrospray ionization may lead to highly charged species for which the charge state resolution is then lacking. On the opposite, producing low charge states of such large species ($e.g.$ using MALDI-MS) results in ions with m/z so large that the detection efficiency is dramatically reduced using conventional technologies. In addition, mass spectra are characterized by a broad envelope without any resolved pattern (see Fig. 1 right panel). Without hypothesis on the average charge of particles, it is then impossible to extract any mass information. One way to overcome this limitation is to measure independently the mass (or more exactly the m/z) and the charge z of each ion. This can be fulfilled by the charge detection mass spectrometry (CDMS) technique. CDMS is based on a very simple concept: an ion passing through a conducting cylinder will induce an image charge (proportional to its charge) on the cylinder. Then the charge of the ion can be determined by measuring the amount of charges flowing to the cylinder. The velocity of the individual incoming ion is then obtained from the cylinder length and from the duration of the image charge signal, corresponding to the ion entering and exiting the tube. The m/z of the ion is determined from its energy and velocity. The mass of each ion is finally obtained from the measured charge z and m/z. In 1995, Fuerstenau and Benner[174]
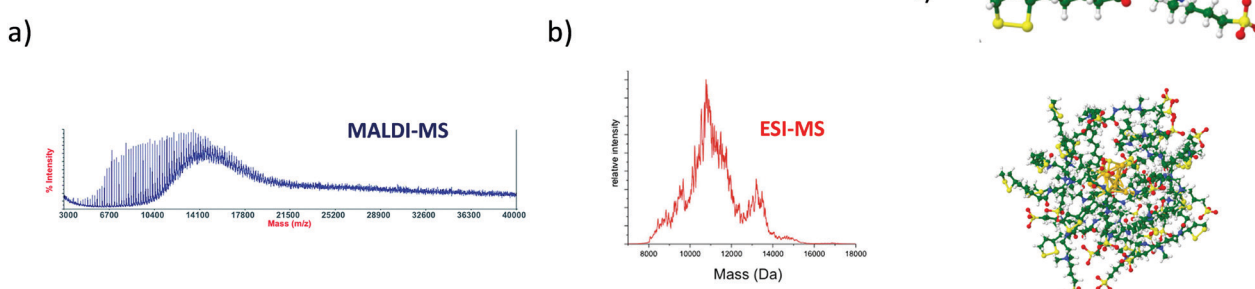

Fig. 5 (a) MALDI-MS and (b) Deconvoluted ESI-MS spectra of gold nanoclusters protected by multi-shells of thioctic bidentate zwitterionic ligands. (c) Possible structure for nanoclusters $Au_{12}Zw_{22}$ (with thioctic-zwitterion ligand (Zw, $C_{15}H_{30}N_2O_4S_3$). Adapted with permission Copyright© © 2017 AIP Publishing and © 2014 and 2019 RSC Publishing).[157,160,257]

coupled CDMS to ESI and really pioneered this technique in analyzing macromolecules in the MDa range, and paved the way to the future studies of biological species and nanoparticles. In more recent years, thanks to the impressive technical developments proposed by the group of Jarrold,[175] CDMS was dramatically improved, enabling the determination of stoichiometry of bio-assemblies. In our group, we were interested in pushing the limits of CDMS for the determination of the mass and charge distribution of very heterogeneous samples containing nanoparticles.[165,176–179] We recently pushed the envelope of characterization of both ligand protected gold nanoclusters and their assembly following zinc-ion-induced aggregation by measuring their entire molar mass distribution by mass spectrometry based methods.[180] Fig. 6b shows the ESI MS spectrum of precursor gold NCs are of stoichiometry $Au_{10}MPA_{10}$ with additional $Au_{11-12}MPA_{11-12}$. Addition of an excess of zinc ions to the as-prepared Au NCs solution, leads to the formation of zinc-mediated complexation reaction-based aggregates of AuNCs for which molar mass information were obtained using charge-detection mass-spectrometry. A mass histogram from the controlled zinc-ion-induced aggregates of AuMPA NCs shows a broad distribution extending from ~75 MDa to more than ~1 GDa, illustrating the ability of CDMS to characterize a large polydispersity of the sub-30 nm nanoparticles. We also

demonstrated the interest of CDMS to characterize gold-thiolate self-assemblies.[178]

3 Couplings

While the above examples have demonstrated the interest in MS as an efficient tool for the mass characterization of ultra-small nanoparticles (and in particular atomically precise nanoclusters), two areas are still not correctly addressed by this technique for their exhaustive analysis: (i) deep insight into their structural motifs and the chemical composition and (ii) exhaustive characterization of mixtures in nanomaterials samples. Interfacing MS with a (offline or online) separation method helps to better discriminate complex samples. Also, no structural information can be drawn from the only mass measurement. Fortunately, techniques like ion mobility–MS (IM-MS) and tandem MS (MS/MS) including photodissociation and action spectroscopy are able to provide structural information.

3.1 Separation techniques

In early works following the Brust method, synthesis led usually to mixtures of ultrasmall nanoparticles or nanoclusters. And clearly, the addition of separation techniques was helpful to
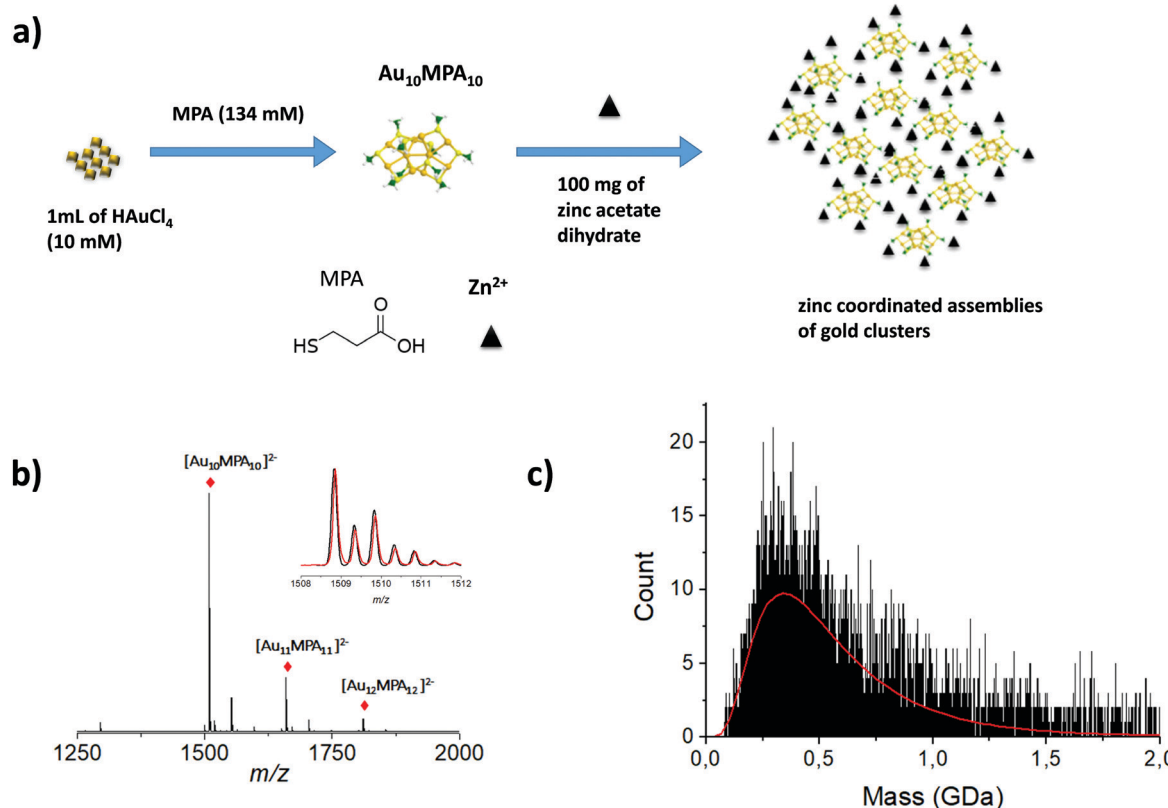

Fig. 6 (a) Schematic illustration of the synthesis process of MPA AuNCs ($Au_{10}MPA_{10}$) adding zinc ion due to trigger aggregation of the MPA AuNCs. (b) Experimentally observed ESI-MS spectrum in negative mode of ionization of Au MPA NCs. Inset: Experimentally observed (red) and simulated (black) ESI-MS isotopic patterns of the 2-charge state of $Au_{10}MPA_{10}$ nanoclusters. (c) Mass histograms for the zinc induced MPA aggregates, obtained by charge-detection mass spectrometry (CDMS) measurements. Experimental distributions are fitted with lognormal distributions (red curve). (Reprinted with permission Copyright© © 2021 RSC Publishing).[180]

exhaustively characterize synthesis products. Polyacrylamide gel electrophoresis (PAGE), high-performance liquid chromatography (HPLC), and thin-layer chromatography (TLC) are the most popular separation methods developed for monolayer protected metal clusters and related clusters. Characterization, analysis, and separation of mixtures of clusters by chromatography have been pioneered by Whetten group.[31–33] A recent review on these techniques applied to thiolate (SR)-protected gold clusters was recently published by Negishi et al.[181] In particular, PAGE was demonstrated to be an efficient technique to separate complex cluster synthesis mixtures prior to ESI-MS analysis (off-line coupling), for which the composition of glutathione protected gold[41] and silver[55,182] nanoclusters was correctly assigned. Size exclusion chromatography has permitted to isolate thiolate-protected gold nanoclusters with core mass of 12 kDa, the collected eluates was then analyzed by ESI-MS to determine the predominant cluster species.[183] Size-dependent electrophoretic migration and separation of water-soluble gold nanoclusters were also obtained by capillary electrophoresis.[184]

HPLC benefits from high resolution and repeatability.[185,186] This technique also has the advantage to be straightforwardly coupled online with electrospray ionization (ESI) mass spectrometry (MS), as opposed to separation by other techniques (PAGE). Thus, it is possible to determine the chemical composition of very minor components that cannot be detected by PAGE. Some of the recent developments include direct coupling of chromatographic techniques to MS. Our group for instance was able to study ultrasmall nanoparticles by combining HPLC and ESI-MS. Time-dependent experiments were conducted on ultrasmall Gd-based silica sub-5 nm nanoparticles aiming at recording both chromatograms and associated mass spectra as a function of time and have permitted to bring new information on the aging processes in such USNPs (as illustrated in Fig. 7).[159] Black et al. coupled reversed-phase chromatography and capillary LC with mass spectrometry and separated gold clusters of varying core sizes from their mixtures.[187–191] As illustrated in Fig. 8, they demonstrated that using volatile trimethylamine as an ion-pair reagent enhances separation of Au_n(m-MBA)$_m$ clusters (m-MBA = m-mercaptobenzoic acid; n = 48–67, m = 26–30), then allowing the determination of their composition.[190]

3.2 Ion mobility-MS

Ion mobility coupled to mass spectrometry (IM-MS) is becoming an indispensable tool for gas phase structural biology.[192–194] In an IM-MS experiment, ions are driven through a buffer gas by a weak electric field, prior to their injection in a mass spectrometer. Ions with different size and shape, or different charges, adopt different velocities in the drift gas and then reach the mass spectrometer at different times. This allows isomer separation before mass measurement. The drift time of the ions can then be converted to a collision cross section (CCS), related to their geometry. IM-MS has been largely applied to study the folding and unfolding mechanisms of proteins.[193] In the field of nanoclusters a significant breakthrough was achieved by Cliffel, McLean and colleagues, who reported the first IM-MS analysis of gold nanoclusters protected by different ligands (tiopronin and
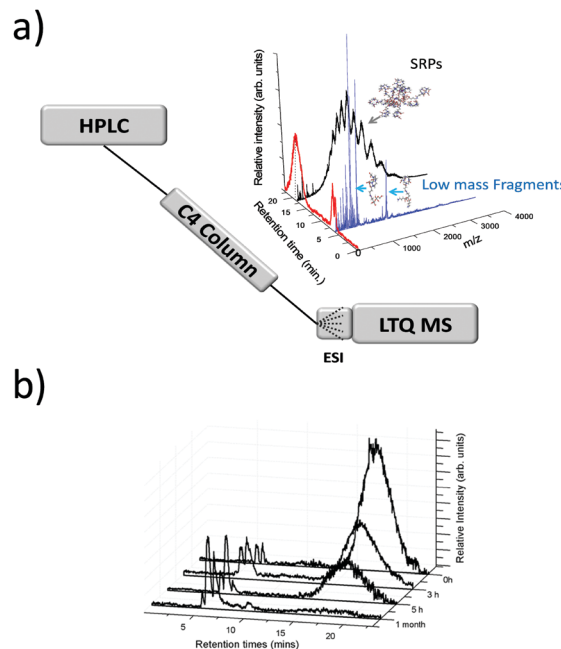

Fig. 7 (a) general online HPLC/ESI-MS setup. HPLC spectrum of the nanoparticles and corresponding mass spectra for each peak of elution (evidencing products of fragmentation and intact small rigid platform SRP NPs. (b) Chromatograms (HPLC-MS) recorded at different aging times of the solution. (reprinted with permission Copyright© 2013 American Chemistry Society).[159]
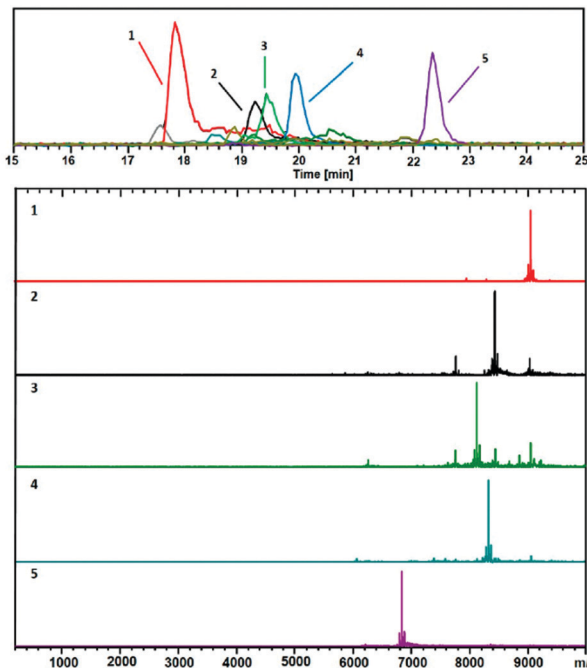
Fig. 8 Positive ESIMS spectra. This analysis shows mainly 2+ charge-states. The black trace corresponds to the base peak chromatogram (m/z 100–10 000). The color-coded EIC chromatographic peaks track with the coded and numbered mass spectra listed herein, with compositions assigned as follows: (1, Red) (67, 30), 18.1 kDa; (2, Black) (60, 31), 16.9 kDa; (3, Green) (58, 30), 16.2 kDa; (4, Blue) (60, 30), 16.6 kDa; and (5, Purple) (48, 26), (13.6 kDa. Reprinted with permission Copyright© 2019 MDPI Publishing).[190]

phenylethanethiolate), as well as gold-tiopronin and gold-phenylethanethiolate precursor complexes.[195] After the pioneering works of Dass *et al.*,[196] who used IM-MS to investigate $Au_{25}(SCH_2CH_2Ph)_{18}$ nanoclusters, the technique has gained importance in the field of protected noble metal NCs. For instance the Pradeep group was very active in IM-MS, figuring out several isomers in ligand protected silver cluster, separating dimers and trimers of $[Au_{25}(SR)_{18}]^-$, looking at the unfolding of lysozyme upon gold addition, probing intercluster reactions or even following oligomerization processes.[153,197–201]

Structural assignment based on IM-MS is nevertheless not as direct and unambiguous as determining the composition of a cluster from a HR-MS measurement. A first step generally consists of generating candidate structures, most often based on molecular modelling. Then, CCS computed for these structures can be compared to the experimental CCS. An important limitation to this procedure is that the CCS is roughly a measure of the average projected surface of the clusters and thus no one-to-one relation exists between structure and CCS. Consequently, a simple match between the CCS of a candidate structure and the experimental value is not sufficient for an assignment. Additional criterion, such as the energetics have to be taken into account. Another challenge to achieve structural assignment

consists of generating the structures. Although force field simulations have often been sufficient for biomolecules, accurate simulations of metallic nanoclusters often require first principle calculations, *e.g.* density functional theory (DFT). Our group reported several studies based on IM-MS, especially applied to the sizing of glutathione-protected gold nanoclusters[202] and to help in structural determination in the case of inorganic nanoclusters.[203] In particular, we investigated homoleptic $Au_{10}SR_{10}$ nanoclusters, for which CCS were measured for different charge states and for different ligands (glutathione as well as smaller thioglycolic acid TGA ligand). For the tripeptide glutathione as ligand, strong charge-state effects on the experimental CCS values were observed and attributed to charge-induced glutathione unfolding. Such a dominant influence of the ligand on the CCS makes it impossible to extract any workable information on the core structure.[204] This effect is nevertheless minimized in the case of smaller and more rigid ligands (such as TGA). In this case, our results supported a possible catenane structure for the cluster, based on comparison with DFT simulations.[205]

Systematic IM-MS studies can also provide information on the influence of ligands on cluster structure, or to investigate their structural stability. For example, the structural changes upon ligand exchange from $[Au_8(PPh_3)_7]^{2+}$ and $[Au_{11}(PPh_3)_9H]^{2+}$
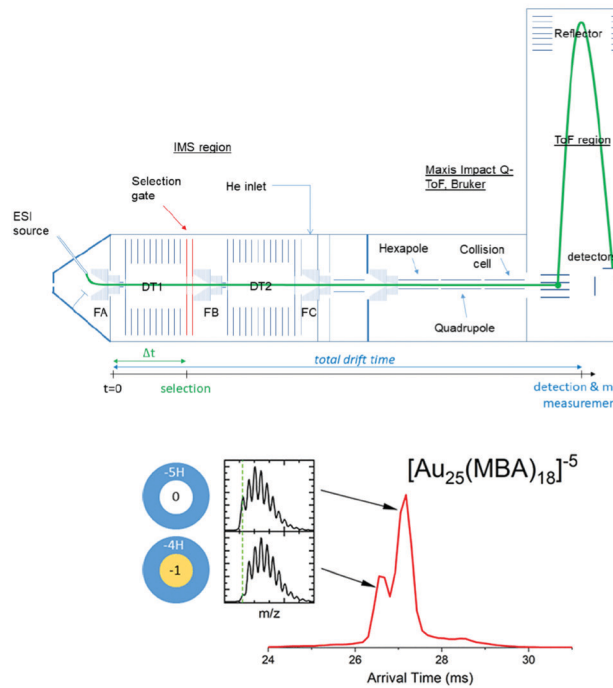
Fig. 9 (left panel) Scheme of the IMS–IMS–MS setup. The green line represents the path of the ions through the instrument, from the electrospray (ESI) ion source transfer capillary. A timeline for IMS–IMS–MS measurements is provided below, where Δt corresponds to the time at which the selection gate is briefly opened (typically for 500 µs) to let through only the ions with a chosen mobility. ATDs for $[Au_{25}\text{-}meta\text{-}MBA_{18}]^{5-}$ clusters with corresponding full isotopic pattern. (right panel) Arrival time distributions extracted for (a) $[Au_{25}\text{-}meta\text{-}MBA_{18}]^{5-}$ clusters and (b) $[Au_{25}\text{-}meta\text{-}MBA_{18}]^{4-}$ clusters by integrating over the full isotopic pattern in each case. Red and green traces were obtained after selection of the ions on the fly (between the two drift tubes), respectively, using the selection windows labeled A and B. These ATDs were normalized to the total ion signal (see text). Corresponding ATDs obtained without selection are also provided as a reference (gray lines). (reprinted with permission Copyright© 2020 American Chemistry Society).[47]
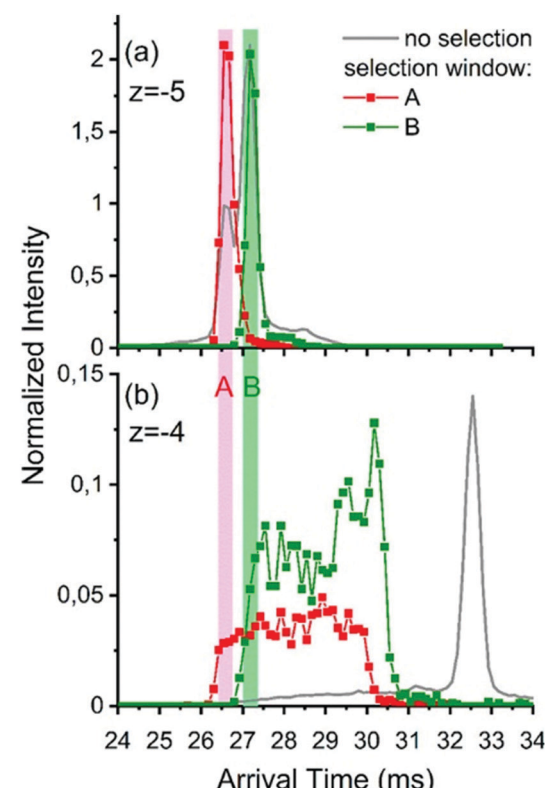
with methyldiphenylphosphine (MePPh$_2$) were evidenced by IM-MS analysis.[206] Recently, Hirata *et al.* studied the effect of collisional excitation on structural properties of nanoclusters and showed that phosphine-protected gold clusters undergo conversion to more compact isomers.[207] Very recently, Hakkinen and coworkers showed that IM-MS was a technique of choice to probe interconversion between isomers of Au$_{25}$(SR)$_{18}$ clusters.[208] Accessible interconversion pathways between the different identified conformers can further be probed by tandem ion mobility measurement (IM–IM–MS), as developed in our group.[209–211] A schematic of the double IMS instrumental setup is presented in Fig. 9. In tandem-ion mobility, a first separation is used to select conformers. Selected ions can then be subjected to collisional activation. Finally, the resulting species are dispersed in the second tube before mass analysis with a time-of-flight mass spectrometer. We used this set-up to investigate the heterogeneity in the charging patterns of Au$_{25}$MBA$_{18}$ clusters. We showed that for a given charge state of those clusters, several populations with different protonation patterns coexist. Part of the observed heterogeneity could be attributed to spontaneous electron loss occurring in the gas phase, which was supported by IM–IM–MS measurements. As illustrated in Fig. 9, we showed that if Au$_{25}$ ions with a 5-charge state are selected at the end of the first drift tube, their drift time in the second drift tube is intermediate between that expected for 5- and 4-ions, suggesting that part of the ions have lost an electron during their flight.[47]

3.3 Dissociation techniques and action spectroscopy

Complementary information regarding the structure and bonding of NCs can be obtained from dissociation studies (tandem MS). The most popular dissociation technique used in mass spectrometry is collision induced dissociation (CID) where mass-selected ions are subjected to energetic collisions with inert gases like Ar, N$_2$, He, *etc.* Several CID studies on ligand-protected NCs were reported. In particular, for Au$_{25}$, common dissociation channels involve surface staple motifs and/or ligand evaporation.[36,55,57,123,143,196,212–214] For larger nanoclusters such as Au$_{144}$(SR)$_{60}$ and Au$_{130}$(SR)$_{50}$, Black *et al.* demonstrated a charge dependence on the extent of fragmentation,[215] as also shown on Au$_{25}$ capped with different isomers of MBA ligands (*ortho*, *meta* and *para*).[216] CID experiments can also be used to probe the relative stability of homologous clusters (by monitoring the energy thresholds for fragmentation). For instance, an isomeric effect of mercaptobenzoic acids on the gas-phase stability of Au$_{25}$(MBA)$_{18}$ NCs was observed. Fig. 10 displays the CID breakdown curves for the 4-charge state of Au$_{25}$(MBA)$_{18}$ for the three isomeric forms of the MBA ligands (ortho (*o*), meta (*m*), and para (*p*)). For *p*-MBA, almost no fragmentation is observed in the explored collision energy range. In contrast, Au$_{25}$ with *o*-MBA ligands appears to be dramatically more sensitive to collisional activation. This was attributed to the different steric hindrance of the carboxylic groups on the ligand shell at the surface of the gold core (higher for m-MBA and, and even more for *o*-MBA). This leads to constraints on the Au–S interface that may reduce the binding energy for fragmentation through Au–S bond

breaking.[216] Surface-induced dissociation (SID), where mass selected ions are collided with Au surfaces protected by mono-layers of alkanethiols was found to be a more convenient technique than CID, as it produce more fragments.[199] It is also better suited to extract thermodynamic parameters of the cluster ions (threshold energies and activation entropies of fragmentation), as demonstrated by Johnson *et al.* on small TPP-protected Au clusters.[217] Recently Brodbelt, Whetten and coworkers evidenced the interest of dissociation techniques using near-vacuum ultraviolet photodissociation.[218] Upon 193 nm irradiation (excitation laser wavelength), high-energy fragmentation pathways and cleavage of Au–S and C–S bonds may be reached, which leads to massive fragmentation (as compared to CID or SID). Interestingly the final products of the fragmentation in this case consist of bare gold cluster ions, which allows to unambiguously determine the size of the cluster core. CID was also used as an efficient tool to produce bare metal clusters, inside[62] and outside[219] mass spectrometers, from sequential evaporation of ligated clusters, as pioneered by our group for producing small silver clusters.[220]
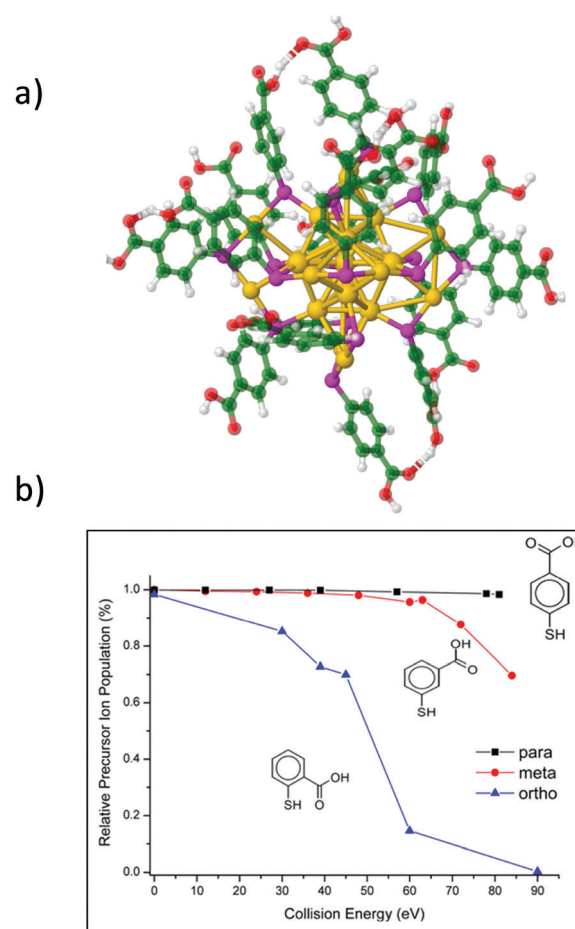
**Fig. 10** (a) Proposed structure for Au$_{25}$(MBA)$_{18}$ with *p*-MBA isomeric ligand. (b) CID breakdown curves for the 4-charge state of Au$_{25}$(MBA)$_{18}$ for the three isomeric MBA ligands as a function of collision energy. (reprinted with permission Copyright© 2018 American Chemistry Society).[216]
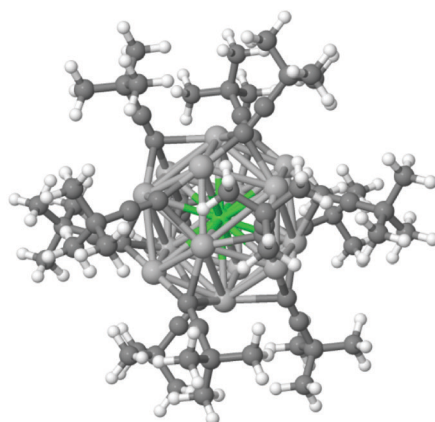
Fig. 11 DFT-optimized structures (chlorine, light green; silver, light gray; copper, orange; carbon, dark green; hydrogen, white) for $[Ag_{14}(C \equiv CtBu)_{12}Cl]^+$ with Ion-mobility arrival times (red peak) and optical action spectra in the UV and VUV range. (reprinted with permission Copyright © 2017 American Chemistry Society).[203]

Of note, upon UV and near-UV irradiation, negatively charged nanoclusters display electron photodetachment as the main observed channel. This channel can be conveniently used either for action spectroscopy or to produce activated radical species that efficiently promotes additional fragmentation.[212,221,222]

Some types of mass spectrometry devices can also act as storage devices (*e.g.* ion trap mass spectrometer). Tunable lasers can be injected within such traps to irradiate a bunch of mass-selected ions. Action spectroscopy then consists of recording the fragmentation (or photodetachment) yields as a function of excitation laser wavelength, thus providing insight into the absorption properties of gas phase ions.[223–226] This coupling leading to action spectroscopy was pioneered by our group to study visible and ultraviolet spectroscopy of gas phase protein ions.[221] We also applied this technique to provide general insight into the nature of electronic excitations at the metal–bioorganic interface[58,227–234] that involve π–π^* excitation within bioorganic subunits, charge transfer between two sub-units and intrametallic excitations.[227] However, more recently, we moved towards a more rational strategy aiming at combining ion mobility on one hand and action spectroscopy on other hand to better determine the structure-optical properties relationship.[203] For instance, $[Ag_{14}(C \equiv CtBu)_{12}Cl]^+$, $[Ag_{14}(C \equiv CtBu)_{12}Br]^+$ were characterized by IM–MS. These cluster ions showed a single peak in ion mobility arrival time distribution and comparison of the CCS values derived from IM with the CCS values modelled from its X-ray crystal structure suggested that the gas-phase structures of the clusters are closely related to their condensed-phase structures (Fig. 11). Then we performed VUV and UV action spectroscopy on $[Ag_{14-n}Cu_n(C \equiv CtBu)_{12}X]^+$ (X = Cl and Br). Thanks to VUV action spectroscopy, the ionization onsets of the cluster ions were determined to be $\sim$8.8 eV. In the UV range, action spectroscopy gave the "absorption" spectra of the cluster ions in the gas phase
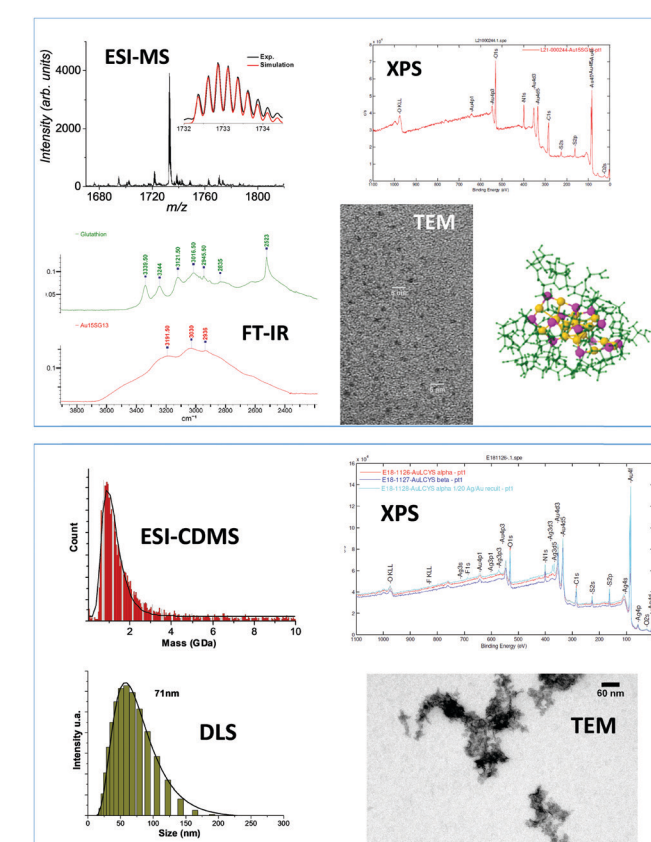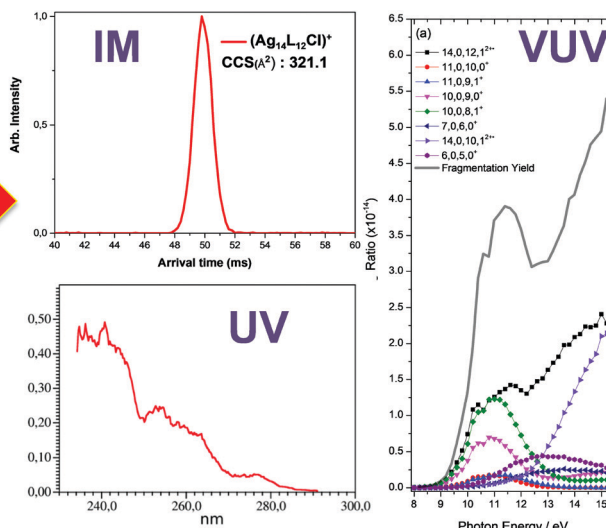
**Fig. 12** Examples of characterization techniques in addition to mass spectrometry used for atomically precise $Au_{15}SG_{13}$ nanoclusters (top panel) and Sub-100 nanometer silver doped gold–cysteine supramolecular assemblies (bottom panel). XPS: X-ray photoelectron spectroscopy, FT-IR: Fourier-transform IR spectroscopy, TEM: Transmission electron miscorscopy, DLS: dynamic light scattering.

(Fig. 11). The experimental optical absorption spectra compared with TDDFT calculations permitted to figure out the key electronic excitations responsible for observed absorption band with a IM-MS characterized structure.[203]

4 Concluding remarks

In this perspective article, we reviewed the current trends in mass spectrometry as a powerful characterization tool for nanomaterials. For nanoclusters produced at the atomic precision, both composition in terms of stoichiometry (between ligands and metal atoms) and charge states of the metal kernel as well as compound evolution during the synthesis can be determined by high-resolution mass spectrometry. Mass spectrometry based tools can be used to weighing ultrasmall nanoparticles in the mass range of few hundreds of kilodalton and for nanoclusters presenting mass dispersion but usually some assumptions on the charge state and on the NP composition are required to obtain information on their composition. The combination of electrospray ionization with multiplicative correlation algorithms was found to be a useful tool for characterization of polydisperse nanoclusters in the mass range 10–100 kDa. For larger molecular weight, e.g. megadalton or even larger, that are observed for self-assembly of precision noble metal nanoclusters, mass information can be fulfilled by the charge detection mass spectrometry technique that directly measures the mass and the charge z of each ion. In particular the recent improvement of charge detection mass spectrometry (using electrostatic storage devices)[175] allows for unprecedented low charge limits and would allow for better insights into the mechanism of formation of large assemblies: from kilodalton individual clusters to their megadalton self assembly.[180] Of note, this mass range appears optimal for nanomechanical resonators[235] like nanomechanical mass spectrometers.[236]

Definitely, mass spectrometry is becoming a technique of profound importance for materials science, and is now an indispensable tool completing the characterization toolbox. Depending on the synthesis routes, information on nanomaterials ranging from its composition at the atomic precision to the estimation of its average mass and distribution can be obtained. It is nevertheless central to keep in mind that mass spectrometry cannot be a single technique with respect to characterization of nanomaterials. Even in the field of atomically precise nanoclusters, a wide range of complementary techniques must be employed for exhaustive nanocluster characterization (as illustrated in Fig. 12).[237–239]

Gas-phase spectroscopy involving electronic excitations in combination with ion mobility has recently gained importance in revealing the structural details and structural dynamics of biomolecular objects.[209–211] In a similar manner, such studies may be extended with gas phase IR (for vibrational excitations) and VUV (for valence shell excitations) spectroscopies in the case of nanoclusters as complement tools for understanding the structures of isomers.[203,240,241] Negatively charged nanoclusters are usually prone to detach electrons upon photoexcitation, and

clearly photoelectron spectroscopy (PES) could be more explored to better address electronic properties of the NCs.[212,242] Also, the coupling between electron photodetachment or PES with circular dichroism[243,244] may be of interest to better understand the chirality in liganded nanoclusters. Indeed, the ionization energies of gold core is ∼7.5 eV while the ionization energies of sulfur-containing ligands are ∼9.5 eV. Thus by playing with the VUV photon energy, it would be possible to decipher the origin of chirality in such nano-objects by recording VUV photoelectron spectroscopy and photoelectron circular dichroism.

Another promising direction may consist of transposing to nanoclusters strategies successfully applied in top-down proteomics, where intact protein ions or large protein fragments are subjected to gas-phase fragmentation before MS analysis. Dissociation techniques and in particular UVPD might allow developing the concept of top-down "metal nanocluster omics". Namely, rich fragmentation patterns such as those which can be produced by 193 nm laser photodissociation,[10,218] could be systematically exploited for the exhaustive characterization of each constituent of the clusters, from the ligands to the core. This is particularly appealing when dealing with complex nanomaterials with mixtures of surface capping ligands or alloy kernels, for which the mass of the whole assembly gives poor information on the stoichiometry of the building blocks.

Beyond pure MS, hyphenated methodologies that combine separation techniques with mass spectrometry are becoming central for materials synthesis, allowing a rapid investigation of complex mixtures in synthetic protocols for materials at the atomic precision. A promising future of such hyphenated techniques for such characterizations will be employing either top-down enzymatic digestion of the proteins bound to the NP surface, and their subsequent separation and identification and/or quantification by separation techniques combined to mass spectrometry or direct analysis by charge detection mass spectrometry might help to follow the "aging" of ultra-small NPs in vitro.[245–247] The aging of USNPs in vitro (or in vivo) remain a challenging issue in nanomedicine.[245–248] For instance, the characterization and a comprehensive picture of the "protein corona" arising after exposure to NPs in cells and organisms might benefit from operando strategies using mass spectrometry imaging.[249]

Finally, electrospray and MALDI are methods of choice for efficiently ionizing nanomaterials and thus for their analysis by MS instruments, but can also be used as source for producing nanomaterials.[250] Indeed, electrospray has shown to be an elegant and versatile way to make a broad array of nanoparticles.[251–253] Combining laser desorption and spray as new "out-of-equilibrium" media will allow for reactivity within droplets and/or laser ablation plume and can lead to new synthetic routes for nanomaterials.[219,254–256]

Conflicts of interest

There are no conflicts to declare.

Notes and references

1 J. J. Thomson, *London, Edinburgh Dublin Philos. Mag. J. Sci.*, 1912, **23**, 449–457.

2 P. F. Knewstubb, 6 - Mass Spectrometry of Ions from Electric Discharges, Flames, and Other Sources, in *Mass Spectrometry of Organic Ions*, ed. F. W. McLafferty, Academic Press, 1963, pp. 255–307.

3 J. Fenn, M. Mann, C. Meng, S. Wong and C. Whitehouse, *Science*, 1989, **246**, 64–71.

4 K. Tanaka, H. Waki, Y. Ido, S. Akita, Y. Yoshida, T. Yoshida and T. Matsuo, *Rapid Commun. Mass Spectrom.*, 1988, **2**, 151–153.

5 M. Karas, D. Bachmann, U. Bahr and F. Hillenkamp, *Int. J. Mass Spectrom. Ion Processes*, 1987, **78**, 53–68.

6 J. B. Fenn, *Angew. Chem., Int. Ed.*, 2003, **42**, 3871–3894.

7 A. Makarov, *Anal. Chem.*, 2000, **72**, 1156–1162.

8 E. S. Hecht, M. Scigelova, S. Eliuk and A. Makarov, Fundamentals and Advances of Orbitrap Mass Spectrometry, in *Encyclopedia of Analytical Chemistry*, ed. R. A. Meyers, 2021, DOI: 10.1002/9780470027318.a9309.pub2.

9 A. W. Jones and H. J. Cooper, *Analyst*, 2011, **136**, 3419–3429.

10 J. S. Brodbelt, L. J. Morrison and I. Santos, *Chem. Rev.*, 2020, **120**, 3328–3380.

11 J. M. Wells and S. A. McLuckey, in *Biological Mass Spectrometry*, ed. A. L. Burlingame, Elsevier Academic Press Inc, San Diego, 2005, vol. 402, pp. 148–185.

12 B. C. Bohrer, S. I. Mererbloom, S. L. Koeniger, A. E. Hilderbrand and D. E. Clemmer, *Annu. Rev. Anal. Chem.*, 2008, **1**, 293–327.

13 X. Huang, H. Liu, D. Lu, Y. Lin, J. Liu, Q. Liu, Z. Nie and G. Jiang, *Chem. Soc. Rev.*, 2021, **50**, 5243–5280.

14 B. H. Kim, M. J. Hackett, J. Park and T. Hyeon, *Chem. Mater.*, 2014, **26**, 59–71.

15 Y. Z. Lu and W. Chen, *Anal. Chem.*, 2015, **87**, 10659–10667.

16 P. Chakraborty and T. Pradeep, *NPG Asia Mater.*, 2019, **11**, 48.

17 T. Chen, Q. Yao, R. R. Nasaruddin and J. Xie, *Angew. Chem., Int. Ed.*, 2019, **58**, 11967–11977.

18 K. M. Harkness, D. E. Cliffel and J. A. McLean, *Analyst*, 2010, **135**, 868–874.

19 R. Jin, Y. Pei and T. Tsukuda, *Acc. Chem. Res.*, 2019, **52**, 1.

20 R. Antoine, *Nanomaterials*, 2020, **10**, 377.

21 T. G. Dietz, M. A. Duncan, D. E. Powers and R. E. Smalley, *J. Chem. Phys.*, 1981, **74**, 6511–6512.

22 M. A. Duncan, *Rev. Sci. Instrum.*, 2012, **83**, 041101.

23 W. D. Knight, K. Clemenger, W. A. de Heer, W. A. Saunders, M. Y. Chou and M. L. Cohen, *Phys. Rev. Lett.*, 1984, **52**, 2141–2143.

24 M. Broyer, *Phys. Scr.*, 1989, **T26**, 84–89.

25 H. W. Kroto, J. R. Heath, S. C. O'Brien, R. F. Curl and R. E. Smalley, *Nature*, 1985, **318**, 162–163.

26 E. A. Rohlfing, D. M. Cox and A. Kaldor, *J. Chem. Phys.*, 1984, **81**, 3322–3330.

27 L. A. Bloomfield, M. E. Geusic, R. R. Freeman and W. L. Brown, *Chem. Phys. Lett.*, 1985, **121**, 33–37.

28 M. F. Jarrold and J. E. Bower, *J. Chem. Phys.*, 1986, **85**, 5373–5375.

29 M. Brust, M. Walker, D. Bethell, D. J. Schiffrin and R. Whyman, *J. Chem. Soc., Chem. Commun.*, 1994, 801–802.

30 R. Antoine, P. F. Brevet, H. H. Girault, D. Bethell and D. J. Schiffrin, *Chem. Commun.*, 1997, 1901–1902.

31 T. G. Schaaff, G. Knight, M. N. Shafigullin, R. F. Borkman and R. L. Whetten, *J. Phys. Chem. B*, 1998, **102**, 10643–10646.

32 R. L. Whetten, J. T. Khoury, M. M. Alvarez, S. Murthy, I. Vezmar, Z. L. Wang, P. W. Stephens, C. L. Cleveland, W. D. Luedtke and U. Landman, *Adv. Mater.*, 1996, **8**, 428–433.

33 T. G. Schaaff, M. N. Shafigullin, J. T. Khoury, I. Vezmar, R. L. Whetten, W. G. Cullen, P. N. First, C. Gutiérrez-Wing, J. Ascensio and M. J. Jose-Yacamán, *J. Phys. Chem. B*, 1997, **101**, 7885–7891.

34 M. M. Alvarez, J. T. Khoury, T. G. Schaaff, M. Shafigullin, I. Vezmar and R. L. Whetten, *Chem. Phys. Lett.*, 1997, **266**, 91–98.

35 C. Kumara, V. R. Jupally and A. Dass, in *Gold Clusters, Colloids and Nanoparticles I*, ed. D. M. P. Mingos, Springer International Publishing, Cham, 2014, pp. 155–187.

36 C. A. Fields-Zinna, J. S. Sampson, M. C. Crowe, J. B. Tracy, J. F. Parker, A. M. deNey, D. C. Muddiman and R. W. Murray, *J. Am. Chem. Soc.*, 2009, **131**, 13844–13851.

37 C. A. Fields-Zinna, R. Sardar, C. A. Beasley and R. W. Murray, *J. Am. Chem. Soc.*, 2009, **131**, 16266–16271.

38 A. C. Templeton, M. P. Wuelfing and R. W. Murray, *Acc. Chem. Res.*, 2000, **33**, 27–36.

39 N. K. Chaki, Y. Negishi, H. Tsunoyama, Y. Shichibu and T. Tsukuda, *J. Am. Chem. Soc.*, 2008, **130**, 8608–8610.

40 P. Maity, H. Tsunoyama, M. Yamauchi, S. H. Xie and T. Tsukuda, *J. Am. Chem. Soc.*, 2011, **133**, 20123–20125.

41 Y. Negishi, K. Nobusada and T. Tsukuda, *J. Am. Chem. Soc.*, 2005, **127**, 5261–5270.

42 H. Tsunoyama and T. Tsukuda, *J. Am. Chem. Soc.*, 2009, **131**, 18216–18217.

43 R. Tsunoyama, H. Tsunoyama, P. Pannopard, J. Limtrakul and T. Tsukuda, *J. Phys. Chem. C*, 2010, **114**, 16004–16009.

44 S. Yamazoe, K. Koyasu and T. Tsukuda, *Acc. Chem. Res.*, 2014, **47**, 816–824.

45 C. Kumara, M. M. Hoque, X. Zuo, D. A. Cullen, R. L. Whetten and A. Dass, *J. Phys. Chem. Lett.*, 2018, **9**, 6825–6832.

46 S. Vergara, U. Santiago, C. Kumara, D. Alducin, R. L. Whetten, M. Jose Yacaman, A. Dass and A. Ponce, *J. Phys. Chem. C*, 2018, **122**, 26733–26738.

47 C. Comby-Zerbino, F. Bertorelle, P. Dugourd, R. Antoine and F. Chirot, *J. Phys. Chem. A*, 2020, **124**, 5840–5848.

48 A. W. Cook and T. W. Hayton, *Acc. Chem. Res.*, 2018, **51**, 2456–2464.

49 J. F. Parker, C. A. Fields-Zinna and R. W. Murray, *Acc. Chem. Res.*, 2010, **43**, 1289–1296.

50 C. Kumara and A. Dass, *Anal. Chem.*, 2014, **86**, 4227–4232.

51 M. Waszkielewicz, J. Olesiak-Banska, C. Comby-Zerbino, F. Bertorelle, X. Dagany, A. K. Bansal, M. T. Sajjad,

I. D. W. Samuel, Z. Sanader, M. Rozycka, M. Wojtas, K. Matczyszyn, V. Bonacic-Koutecky, R. Antoine, A. Ozyhar and M. Samoc, *Nanoscale*, 2018, **10**, 11335–11341.

52 L. G. AbdulHalim, S. Ashraf, K. Katsiev, A. R. Kirmani, N. Kothalawala, D. H. Anjum, S. Abbas, A. Amassian, F. Stellacci, A. Dass, I. Hussain and O. M. Bakr, *J. Mater. Chem. A*, 2013, **1**, 10148–10154.

53 I. Chakraborty and T. Pradeep, *Chem. Rev.*, 2017, **117**, 8208–8271.

54 R. Jin, C. Zeng, M. Zhou and Y. Chen, *Chem. Rev.*, 2016, **116**, 10346–10413.

55 F. Bertorelle, R. Hamouda, D. Rayane, M. Broyer, R. Antoine, P. Dugourd, L. Gell, A. Kulesza, R. Mitric and V. Bonacic-Koutecky, *Nanoscale*, 2013, **5**, 5637–5643.

56 W. H. Ding, L. M. Guan, J. J. Han, R. Mangala and Z. X. Luo, *Sens. Actuators, B*, 2017, **250**, 364–371.

57 B. Bellina, I. Compagnon, F. Bertorelle, M. Broyer, R. Antoine, P. Dugourd, L. Gell, A. Kulesza, R. Mitric and V. Bonacic-Koutecky, *J. Phys. Chem. C*, 2011, **115**, 24549–24554.

58 V. Bonacic-Koutecky, A. Kulesza, L. Gell, R. Mitric, R. Antoine, F. Bertorelle, R. Hamouda, D. Rayane, M. Broyer, T. Tabarin and P. Dugourd, *Phys. Chem. Chem. Phys.*, 2012, **14**, 9282–9290.

59 I. Russier-Antoine, F. Bertorelle, N. Calin, Z. Sanader, M. Krstic, C. Comby-Zerbino, P. Dugourd, P. F. Brevet, V. Bonacic-Koutecky and R. Antoine, *Nanoscale*, 2017, **9**, 1221–1228.

60 I. Russier-Antoine, F. Bertorelle, R. Hamouda, D. Rayane, P. Dugourd, Z. Sanader, V. Bonacic-Koutecky, P.-F. Brevet and R. Antoine, *Nanoscale*, 2016, **8**, 2892–2898.

61 Z. Sanader, M. Krstic, I. Russier-Antoine, F. Bertorelle, P. Dugourd, P. F. Brevet, R. Antoine and V. Bonacic-Koutecky, *Phys. Chem. Chem. Phys.*, 2016, **18**, 12404–12408.

62 A. Ghosh, M. Bodiuzzaman, A. Nag, M. Jash, A. Baksi and T. Pradeep, *ACS Nano*, 2017, **11**, 11145–11151.

63 X. Y. Ma, Y. Lv, H. Li, T. Chen, J. Zeng, M. Z. Zhu and H. Z. Yu, *J. Phys. Chem. C*, 2020, **124**, 13421–13426.

64 N. Xia, J. Yang and Z. K. Wu, *Nanoscale*, 2015, **7**, 10013–10020.

65 F. L. Bi, H. Q. Yin, S. Y. Zheng, Q. H. Zhu, H. F. Yang, M. Kang, F. Gan and X. J. Chen, *RSC Adv.*, 2016, **6**, 4627–4633.

66 H. Kawasaki, H. Yamamoto, H. Fujimori, R. Arakawa, Y. Iwasaki and M. Inada, *Langmuir*, 2010, **26**, 5926–5933.

67 P. Gao, H. Wang, G. F. Zou and K. Q. Zhang, *RSC Adv.*, 2018, **8**, 27805–27810.

68 D. Q. Feng, G. L. Liu and W. Wang, *J. Mater. Chem. B*, 2015, **3**, 2083–2088.

69 G. Y. Lan, W. Y. Chen and H. T. Chang, *Analyst*, 2011, **136**, 3623–3628.

70 G. Y. Lan, W. Y. Chen and H. T. Chang, *RSC Adv.*, 2011, **1**, 802–807.

71 J. Lee, J. Park, H. H. Lee, H. Park, H. I. Kim and W. J. Kim, *Biosens. Bioelectron.*, 2015, **68**, 642–647.

72 K. Morishita, J. L. MacLean, B. W. Liu, H. Jiang and J. W. Liu, *Nanoscale*, 2013, **5**, 2840–2849.

73 S. Jin, W. J. Du, S. X. Wan, X. Kang, M. Chen, D. Q. Hu, S. Chen, X. J. Zou, G. D. Sun and M. Z. Zhu, *Inorg. Chem.*, 2017, **56**, 11151–11159.

74 S. Jin, F. Q. Xu, W. J. Du, X. Kang, S. Chen, J. Zhang, X. W. Li, D. Q. Hu, S. X. Wang and M. Z. Zhu, *Inorg. Chem.*, 2018, **57**, 5114–5119.

75 T. K. Chen and J. P. Xie, *Chem. Rec.*, 2016, **16**, 1761–1771.

76 Q. F. Yao, Y. Yu, X. Yuan, Y. Yu, J. P. Xie and J. Y. Lee, *Small*, 2013, **9**, 2696–2701.

77 Q. F. Yao, X. Yuan, Y. Yu, Y. Yu, J. P. Xie and J. Y. Lee, *J. Am. Chem. Soc.*, 2015, **137**, 2128–2136.

78 X. Yuan, N. Goswami, W. Chen, Q. Yao and J. Xie, *Chem. Commun.*, 2016, **52**, 5234–5237.

79 J. Chen, Q. F. Zhang, T. A. Bonaccorso, P. G. Williard and L. S. Wang, *J. Am. Chem. Soc.*, 2014, **136**, 92–95.

80 S. Maity, D. Bain and A. Patra, *J. Phys. Chem. C*, 2019, **123**, 2506–2515.

81 R. W. Huang, J. Yin, C. W. Dong, A. Ghosh, M. J. Alhilaly, X. L. Dong, M. N. Hedhili, E. Abou-Hamad, B. Alamer, S. Nematulloev, Y. Han, O. F. Mohammed and O. M. Bakr, *J. Am. Chem. Soc.*, 2020, **142**, 8696–8705.

82 X. H. Gao, C. Du, C. M. Zhang and W. Chen, *ChemElectroChem*, 2016, **3**, 1266–1272.

83 S. K. Barik, S. C. Huo, C. Y. Wu, T. H. Chiu, J. H. Liao, X. P. Wang, S. Kahlal, J. Y. Saillard and C. W. Liu, *Chem. – Eur. J.*, 2020, **26**, 10471–10479.

84 K. K. Chakrahari, R. P. B. Silalahi, T. H. Chiu, X. P. Wang, N. Azrou, S. Kahlal, Y. C. Liu, M. H. Chiang, J. Y. Saillard and C. W. Liu, *Angew. Chem., Int. Ed.*, 2019, **58**, 4943–4947.

85 A. W. Cook, Z. R. Jones, G. Wu, S. J. Teat, S. L. Scott and T. W. Hayton, *Inorg. Chem.*, 2019, **58**, 8739–8749.

86 K. Basu, K. Gayen, T. Mitra, A. Baral, S. S. Roy and A. Banerjee, *ChemNanoMat*, 2017, **3**, 808–814.

87 M. Zhu, S. M. Zhou, C. H. Yao, L. W. Liao and Z. K. Wu, *Nanoscale*, 2014, **6**, 14195–14199.

88 Y. Z. Pan, J. S. Chen, S. D. Gong and Z. H. Wang, *Dalton Trans.*, 2018, **47**, 11097–11103.

89 K. S. Joya, L. Sinatra, L. G. AbdulHalim, C. P. Joshi, M. N. Hedhili, O. M. Bakr and I. Hussain, *Nanoscale*, 2016, **8**, 9695–9703.

90 A. W. Cook, G. Wu and T. W. Hayton, *Inorg. Chem.*, 2018, **57**, 8189–8194.

91 P. K. Aneesh, C. Govind and S. R. Nambiar, *Anal. Methods*, 2019, **11**, 2089–2096.

92 S. Dolai, A. Dass and R. Sardar, *Langmuir*, 2013, **29**, 6187–6193.

93 X. Kang, Y. Li, M. Zhu and R. Jin, *Chem. Soc. Rev.*, 2020, **49**, 6443–6514.

94 D. Mishra, V. Lobodin, C. Q. Zhang, F. Aldeek, E. Lochner and H. Mattoussi, *Phys. Chem. Chem. Phys.*, 2018, **20**, 12992–13007.

95 G. Soldan, M. A. Aljuhani, M. S. Bootharaju, L. G. AbdulHalim, M. R. Parida, A. H. Emwas, O. F. Mohammed and O. M. Bakr, *Angew. Chem., Int. Ed.*, 2016, **55**, 5749–5753.

96 M. van der Linden, A. J. van Bunningen, L. Amidani, M. Bransen, H. Elnaggar, P. Glatzel, A. Meijerink and F. M. F. de Groot, *ACS Nano*, 2018, **12**, 12751–12760.

97 M. van der Linden, A. J. van Bunningen, M. U. Delgado-Jaime, B. Detlefs, P. Glatzel, A. Longo and F. M. F. de Groot, *J. Phys. Chem. C*, 2018, **122**, 28351–28361.

98 X. Kang, X. Wei, S. Jin, Q. Yuan, X. Luan, Y. Pei, S. Wang, M. Zhu and R. Jin, *Proc. Natl. Acad. Sci. U. S. A.*, 2019, **116**, 18834–18840.

99 B. Zhang, G. Salassa and T. Burgi, *Chem. Commun.*, 2016, **52**, 9205–9207.

100 C. Yao, J. Chen, M.-B. Li, L. Liu, J. Yang and Z. Wu, *Nano Lett.*, 2015, **15**, 1281–1287.

101 C. Kumara, X. Zuo, D. A. Cullen and A. Dass, *J. Phys. Chem. Lett.*, 2015, **6**, 3320–3326.

102 J. Fan, Y. Song, J. Chai, S. Yang, T. Chen, B. Rao, H. Yu and M. Zhu, *Nanoscale*, 2016, **8**, 15317–15322.

103 S. Wang, X. Meng, A. Das, T. Li, Y. Song, T. Cao, X. Zhu, M. Zhu and R. Jin, *Angew. Chem., Int. Ed.*, 2014, **53**, 2376–2380.

104 H. F. Qian, B. Ellen, Y. Zhu and R. C. Jin, *Acta Phys.-Chim. Sin.*, 2011, **27**, 513–519.

105 J. S. Chen, L. R. Liu, X. Liu, L. W. Liao, S. L. Zhuang, S. M. Zhou, J. L. Yang and Z. K. Wu, *Chem. – Eur. J.*, 2017, **23**, 18187–18192.

106 X. Kang, F. Q. Xu, X. Wei, S. X. Wang and M. Z. Zhu, *Sci. Adv.*, 2019, **5**, eaax7863.

107 Y. Niihori, W. Kurashige, M. Matsuzaki and Y. Negishi, *Nanoscale*, 2013, **5**, 508–512.

108 M. S. Bootharaju, S. M. Kozlov, Z. Cao, M. Harb, M. R. Parida, M. N. Hedhili, O. F. Mohammed, O. M. Bakr, L. Cavallo and J. M. Basset, *Nanoscale*, 2017, **9**, 9529–9536.

109 H. Gholipour-Ranjbar, H. Fang, J. Guan, D. A. Peters, A. Seifert, P. Jena and J. Laskin, *Small*, 2020, 2002927.

110 E. Khatun, P. Chakraborty, B. R. Jacob, G. Paramasivam, M. Bodiuzzaman, W. A. Dar and T. Pradeep, *Chem. Mater.*, 2020, **32**, 611–619.

111 M. S. Bootharaju, S. M. Kozlov, Z. Cao, A. Shkurenko, A. M. El-Zohry, O. F. Mohammed, M. Eddaoudi, O. M. Bakr, L. Cavallo and J. M. Basset, *Chem. Mater.*, 2018, **30**, 2719–2725.

112 M. S. Bootharaju, L. Sinatra and O. M. Bakr, *Nanoscale*, 2016, **8**, 17333–17339.

113 P. Bose, P. Chakraborty, J. S. Mohanty, Nonappa, A. R. Chowdhuri, E. Khatun, T. Ahuja, A. Mahendranath and T. Pradeep, *Nanoscale*, 2020, **12**, 22116–22128.

114 K. Y. Zheng, V. Fung, X. Yuan, D. E. Jiang and J. P. Xie, *J. Am. Chem. Soc.*, 2019, **141**, 18977–18983.

115 M. Neumaier, A. Baksi, P. Weis, E. K. Schneider, P. Chakraborty, H. Hahn, T. Pradeep and M. M. Kappes, *J. Am. Chem. Soc.*, 2021, **143**, 6969–6980.

116 J. B. Tracy, M. C. Crowe, J. F. Parker, O. Hampe, C. A. Fields-Zinna, A. Dass and R. W. Murray, *J. Am. Chem. Soc.*, 2007, **129**, 16209–16215.

117 A. Dass, K. Holt, J. F. Parker, S. W. Feldberg and R. W. Murray, *J. Phys. Chem. C*, 2008, **112**, 20276–20283.

118 S. Hossain, W. Kurashige, S. Wakayama, B. Kumar, L. V. Nair, Y. Niihori and Y. Negishi, *J. Phys. Chem. C*, 2016, **120**, 25861–25869.

119 X. M. Meng, Q. Xu, S. X. Wang and M. Z. Zhu, *Nanoscale*, 2012, **4**, 4161–4165.

120 Y. A. Attia and S. H. Abdel-Hafez, *New J. Chem.*, 2018, **42**, 9606–9611.

121 W. Kurashige, S. Yamazoe, K. Kanehira, T. Tsukuda and Y. Negishi, *J. Phys. Chem. Lett.*, 2013, **4**, 3181–3185.

122 Y. Cao, V. Fung, Q. Yao, T. Chen, S. Zang, D.-E. Jiang and J. Xie, *Nat. Commun.*, 2020, **11**, 5498.

123 G. E. Johnson and J. Laskin, *Analyst*, 2016, **141**, 3573–3589.

124 M. P. Maman, A. S. Nair, H. Cheraparambil, B. Pathak and S. Mandal, *J. Phys. Chem. Lett.*, 2020, **11**, 1781–1788.

125 A. Kim, C. J. Zeng, M. Zhou and R. C. Jin, *Part. Part. Syst. Charact.*, 2017, **34**, 1600388.

126 Z. Huang, Y. Ishida, K. Narita and T. Yonezawa, *J. Phys. Chem. C*, 2018, **122**, 18142–18150.

127 Y. T. Cao, J. H. Guo, R. Shi, G. I. N. Waterhouse, J. H. Pan, Z. X. Du, Q. F. Yao, L. Z. Wu, C. H. Tung, J. P. Xie and T. R. Zhang, *Nat. Commun.*, 2018, **9**, 2379.

128 M. Z. Zhu, G. R. Chan, H. F. Qian and R. C. Jin, *Nanoscale*, 2011, **3**, 1703–1707.

129 L. Tang, X. Kang, S. X. Wang and M. Z. Zhu, *Langmuir*, 2019, **35**, 12350–12355.

130 Q. F. Yao, V. Fung, C. Sun, S. D. Huang, T. K. Chen, D. E. Jiang, J. Y. Lee and J. P. Xie, *Nat. Commun.*, 2018, 9.

131 R. R. Nasaruddin, Q. F. Yao, T. K. Chen, M. J. Hulsey, N. Yan and J. P. Xie, *Nanoscale*, 2018, **10**, 23113–23121.

132 Y. Yu, Z. T. Luo, Y. Yu, J. Y. Lee and J. P. Xie, *ACS Nano*, 2012, **6**, 7920–7927.

133 G. Li, H. Abroshan, Y. X. Chen, R. C. Jin and H. J. Kim, *J. Am. Chem. Soc.*, 2015, **137**, 14295–14304.

134 L. Yang, H. Cheng, Y. Jiang, T. Huang, J. Bao, Z. Sun, Z. Jiang, J. Ma, F. Sun, Q. Liu, T. Yao, H. Deng, S. Wang, M. Zhu and S. Wei, *Nanoscale*, 2015, **7**, 14452–14459.

135 A. C. Dharmaratne, T. Krick and A. Dass, *J. Am. Chem. Soc.*, 2009, **131**, 13604–13605.

136 R. Jin, G. Li, S. Sharma, Y. Li and X. Du, *Chem. Rev.*, 2021, **121**, 567–648.

137 Y. Lu, Y. Jiang, X. Gao and W. Chen, *Chem. Commun.*, 2014, **50**, 8464–8467.

138 S. Antonello, N. V. Perera, M. Ruzzi, J. A. Gascón and F. Maran, *J. Am. Chem. Soc.*, 2013, **135**, 15585–15594.

139 A. Venzo, S. Antonello, J. A. Gascón, I. Guryanov, R. D. Leapman, N. V. Perera, A. Sousa, M. Zamuner, A. Zanella and F. Maran, *Anal. Chem.*, 2011, **83**, 6355–6362.

140 Z. Wu, C. Gayathri, R. R. Gil and R. Jin, *J. Am. Chem. Soc.*, 2009, **131**, 6535–6542.

141 R. C. Jin, *Nanoscale*, 2015, **7**, 1549–1565.

142 Y. Negishi, N. K. Chaki, Y. Shichibu, R. L. Whetten and T. Tsukuda, *J. Am. Chem. Soc.*, 2007, **129**, 11322–11323.

143 R. Hamouda, F. Bertorelle, D. Rayane, R. Antoine, M. Broyer and P. Dugourd, *Int. J. Mass Spectrom.*, 2013, **335**, 1–6.

144 A. Dass, S. Theivendran, P. R. Nimmala, C. Kumara, V. R. Jupally, A. Fortunelli, L. Sementa, G. Barcaro,

X. Zuo and B. C. Noll, *J. Am. Chem. Soc.*, 2015, **137**, 4610–4613.

145 Q. Z. Li, J. S. Chai, S. Yang, Y. B. Song, T. Chen, C. Chen, H. Zhang, H. Z. Yu and M. Z. Zhu, *Small*, 2020, 1907114.

146 N. Fernández-Iglesias and J. Bettmer, *Nanoscale*, 2014, **6**, 716–721.

147 M. Kluz, H. Nieznańska, R. Dec, I. Dzięcielewski, B. Niżyński, G. Ścibisz, W. Puławski, G. Staszczak, E. Klein, J. Smalc-Koziorowska and W. Dzwolak, *PLoS One*, 2019, **14**, e0218975.

148 J. Xie, Y. Zheng and J. Y. Ying, *J. Am. Chem. Soc.*, 2009, **131**, 888–889.

149 T. Pradeep, A. Baksi and P. L. Xavier, *Functional Nanometer-Sized Clusters of Transition Metals: Synthesis, Properties and Applications*, The Royal Society of Chemistry, 2014, pp. 169–225.

150 H. Kouchi, H. Kawasaki and R. Arakawa, *Anal. Methods*, 2012, **4**, 3600–3603.

151 D. Ghosh, S. K. Mudedla, M. R. Islam, V. Subramanian and T. Pradeep, *J. Phys. Chem. C*, 2019, **123**, 17598–17605.

152 D. Ghosh, M. Bodiuzzaman, A. Som, S. Raja, A. Baksi, A. Ghosh, J. Ghosh, A. Ganesh, P. Samji, S. Mahalingam, D. Karunagaran and T. Pradeep, *J. Phys. Chem. C*, 2019, **123**, 29408–29417.

153 D. Ghosh, A. Baksi, S. K. Mudedla, A. Nag, M. A. Ganayee, V. Subramanian and T. Pradeep, *J. Phys. Chem. C*, 2017, **121**, 13335–13344.

154 K. Chaudhari, P. L. Xavier and T. Pradeep, *ACS Nano*, 2011, **5**, 8816–8827.

155 Y. C. Hsu, M. J. Hung, Y. A. Chen, T. F. Wang, Y. R. Ou and S. H. Chen, *Molecules*, 2019, **24**, 1630.

156 Y. Zhang, M. F. Yan, S. B. Wang, J. J. Jiang, P. F. Gao, G. M. Zhang, C. Dong and S. M. Shuang, *RSC Adv.*, 2016, **6**, 8612–8619.

157 X. L. Guevel, O. Tagit, C. E. Rodríguez, V. Trouillet, M. Pernia Leal and N. Hildebrandt, *Nanoscale*, 2014, **6**, 8091–8099.

158 R. Antoine, C. Truillet, P. Dugourd, F. Lux and O. Tillement, *France Pat.*, FR3010527A1, 2015.

159 C. Truillet, F. Lux, O. Tillement, P. Dugourd and R. Antoine, *Anal. Chem.*, 2013, **85**, 10440–10447.

160 D. J. Shen, M. Henry, V. Trouillet, C. Comby-Zerbino, F. Bertorelle, L. Sancey, R. Antoine, J. L. Coll, V. Josserand and X. Le Guevel, *APL Mater.*, 2017, **5**, 053404.

161 C. Colombe, X. Le Guevel, A. Martin-Serrano, M. Henry, E. Porret, C. Comby-Zerbino, R. Antoine, I. Atallah, B. Busser, J. L. Coll, C. A. Righini and L. Sancey, *Nanomedicine*, 2019, **20**, 102011.

162 B. Musnier, K. D. Wegner, C. Comby-Zerbino, V. Trouillet, M. Jourdan, I. Hausler, R. Antoine, J. L. Coll, U. Resch-Genger and X. Le Guevel, *Nanoscale*, 2019, **11**, 12092–12096.

163 E. Porret, M. Jourdan, B. Gennaro, C. Comby-Zerbino, F. Bertorelle, V. Trouillet, X. Qiu, C. Zoukimian, D. Boturyn, N. Hildebrandt, R. Antoine, J. L. Coll and X. Le Guavel, *J. Phys. Chem. C*, 2019, **123**, 26705–26717.

164 A. R. Ziefuss, T. Steenbock, D. Benner, A. Plech, J. Göttlicher, M. Teubner, C. Rehbock, C. Comby-Zerbino, R. Antoine, D. Amans, I. Chakraborty, G. Bester, B. Sures, M. Rübhausen, W. J. Parak and S. Barcikwoski, *Adv. Mater.*, 2021, DOI: 10.1002/adma.202101549.

165 M. Loumaigne, C. Midelet, T. Doussineau, P. Dugourd, R. Antoine, M. Stamboul, A. Debarre and M. H. V. Werts, *Nanoscale*, 2016, **8**, 6555–6570.

166 F. Lux, A. Mignot, P. Mowat, C. Louis, S. Dufort, C. Bernhard, F. Denat, F. Boschetti, C. Brunet, R. Antoine, P. Dugourd, S. Laurent, L. V. Elst, R. Muller, L. Sancey, V. Josserand, J.-L. Coll, V. Stupar, E. Barbier, C. Remy, A. Broisat, C. Ghezzi, D. G. Le, S. Roux, P. Perriat and O. Tillement, *Angew. Chem., Int. Ed.*, 2011, **50**, 12299–12303.

167 A. Mignot, C. Truillet, F. Lux, L. Sancey, C. Louis, F. Denat, F. Boschetti, L. Bocher, A. Gloter, O. Stéphan, R. Antoine, P. Dugourd, D. Luneau, G. Novitchi, L. C. Figueiredo, P. C. de Morais, L. Bonneviot, B. Albela, F. Ribot, L. Van Lokeren, I. Déchamps-Olivier, F. Chuburu, G. Lemercier, C. Villiers, P. N. Marche, G. Le Duc, S. Roux, O. Tillement and P. Perriat, *Chem. – Eur. J.*, 2013, **19**, 6122–6136.

168 J. Morlieras, J. M. Chezal, E. Miot-Noirault, A. Roux, L. Heinrich-Balard, R. Cohen, S. Tarrit, C. Truillet, A. Mignot, R. Hachani, D. Kryza, R. Antoine, P. Dugourd, P. Perriat, M. Janier, L. Sancey, F. Lux and O. Tillement, *Nanoscale*, 2013, **5**, 1603–1615.

169 J. Morlieras, J.-M. Chezal, E. Miot-Noirault, A. Vidal, S. Besse, D. Kryza, C. Truillet, A. Mignot, R. Antoine, P. Dugourd, F. Redini, L. Sancey, F. Lux, P. Perriat, M. Janier and O. Tillement, *Chem. Commun.*, 2013, **49**, 3046–3048.

170 J. Morlieras, S. Dufort, L. Sancey, C. Truillet, A. Mignot, F. Rossetti, M. Dentamaro, S. Laurent, L. Vander Elst, R. N. Muller, R. Antoine, P. Dugourd, S. P. Roux, P. Perriat, F. O. Lux, J.-L. Coll and O. Tillement, *Bioconjugate Chem.*, 2013, **24**, 1584–1597.

171 L. Sancey, S. Kotb, C. Truillet, F. Appaix, A. Marais, E. S. Thomas, B. van der Sanden, J.-P. Klein, B. Laurent, M. L. Cottier, R. Antoine, P. Dugourd, G. R. Panczer, F. O. Lux, P. Perriat, V. Motto-Ros and O. Tillement, *ACS Nano*, 2015, **9**, 2477–2488.

172 V.-L. Tran, V. Thakare, F. Rossetti, A. Baudouin, G. Ramniceanu, B.-T. Doan, N. Mignet, C. Comby-Zerbino, R. Antoine, P. Dugourd, F. Boschetti, F. Denat, C. Louis, S. Roux, T. Doussineau, O. Tillement and F. Lux, *J. Mater. Chem. B*, 2018, **6**, 4821–4834.

173 C. Truillet, F. Lux, J. Moreau, M. Four, L. Sancey, S. Chevreux, G. Boeuf, P. Perriat, C. Frochot, R. Antoine, P. Dugourd, C. Portefaix, C. Hoeffel, M. Barberi-Heyob, C. Terryn, L. van Gulick, G. Lemercier and O. Tillement, *Dalton Trans.*, 2013, **42**, 12410–12420.

174 S. D. Fuerstenau and W. H. Benner, *Rapid Commun. Mass Spectrom.*, 1995, **9**, 1528–1538.

175 D. Z. Keifer, E. E. Pierson and M. F. Jarrold, *Analyst*, 2017, **142**, 1654–1671.

176 R. Antoine, *Rapid Commun. Mass Spectrom.*, 2020, 34, e8539.

177 T. Doussineau, A. Désert, O. Lambert, J.-C. Taveau, M. Lansalot, P. Dugourd, E. Bourgeat-Lami, S. Ravaine, E. Duguet and R. Antoine, *J. Phys. Chem. C*, 2015, 119, 10844–10849.

178 H. Fakhouri, M. Perić, F. Bertorelle, P. Dugourd, X. Dagany, I. Russier-Antoine, P.-F. Brevet, V. Bonačić-Koutecký and R. Antoine, *Phys. Chem. Chem. Phys.*, 2019, 21, 12091–12099.

179 I. Russier-Antoine, H. Fakhouri, S. Basu, F. Bertorelle, P. Dugourd, P.-F. Brevet, P. Velayudhan, S. Thomas, N. Kalarikkal and R. Antoine, *Chem. Commun.*, 2020, 56, 3859–3862.

180 S. Basu, H. Fakhouri, C. Moulin, S. Dolai, I. Russier-Antoine, P.-F. Brevet, R. Antoine and A. Paul, *Nanoscale*, 2021, 13, 4439–4443.

181 Y. Negishi, S. Hashimoto, A. Ebina, K. Hamada, S. Hossain and T. Kawawaki, *Nanoscale*, 2020, 12, 8017–8039.

182 B. Bhattarai, Y. Zaker, A. Atnagulov, B. Yoon, U. Landman and T. P. Bigioni, *Acc. Chem. Res.*, 2018, 51, 3104–3113.

183 H. Qian and R. Jin, *Chem. Commun.*, 2011, 47, 11462–11464.

184 T. Wan, F. L. Tang, Y. R. Yin, M. X. Zhang, M. M. F. Choi and X. P. Yang, *Electrophoresis*, 2019, 40, 1345–1352.

185 S. P. Xie, M. C. Paau, Y. Zhang, S. M. Shuang, W. Chan and M. M. F. Choi, *Nanoscale*, 2012, 4, 5325–5332.

186 Y. Zhang, Q. Hu, M. C. Paau, S. P. Xie, P. F. Gao, W. Chan and M. M. F. Choi, *J. Phys. Chem. C*, 2013, 117, 18697–18708.

187 D. M. Black, M. M. Alvarez, F. Z. Yan, W. P. Griffith, G. Plascencia-Villa, S. B. H. Bach and R. L. Whetten, *J. Phys. Chem. C*, 2017, 121, 10851–10857.

188 D. M. Black, S. B. H. Bach and R. L. Whetten, *Anal. Chem.*, 2016, 88, 5631–5636.

189 D. M. Black, N. Bhattarai, S. B. H. Bach and R. L. Whetten, *J. Phys. Chem. Lett.*, 2016, 7, 3199–3205.

190 D. M. Black, M. M. Hoque, G. Plascencia-Villa and R. L. Whetten, *Nanomaterials*, 2019, 9, 1303.

191 D. M. Black, G. Robles, P. Lopez, S. B. H. Bach, M. Alvarez and R. L. Whetten, *Anal. Chem.*, 2018, 90, 2010–2017.

192 E. Jurneczko and P. E. Barran, *Analyst*, 2011, 136, 20–28.

193 J. L. P. Benesch and B. T. Ruotolo, *Curr. Opin. Struct. Biol.*, 2011, 21, 641–649.

194 T. M. Allison, P. Barran, S. Cianférani, M. T. Degiacomi, V. Gabelica, R. Grandori, E. G. Marklund, T. Menneteau, L. G. Migas, A. Politis, M. Sharon, F. Sobott, K. Thalassinos and J. L. P. Benesch, *Anal. Chem.*, 2020, 92, 10872–10880.

195 K. M. Harkness, L. S. Fenn, D. E. Cliffel and J. A. McLean, *Anal. Chem.*, 2010, 82, 3061–3066.

196 L. A. Angel, L. T. Majors, A. C. Dharmaratne and A. Dass, *ACS Nano*, 2010, 4, 4691–4700.

197 A. Baksi, P. Chakraborty, S. Bhat, G. Natarajan and T. Pradeep, *Chem. Commun.*, 2016, 52, 8397–8400.

198 A. Baksi, E. K. Schneider, P. Weis, K. R. Krishnadas, D. Ghosh, H. Hahn, T. Pradeep and M. M. Kappes, *J. Phys. Chem. C*, 2019, 123, 28477–28485.

199 A. Baksi, S. R. Harvey, G. Natarajan, V. H. Wysocki and T. Pradeep, *Chem. Commun.*, 2016, 52, 3805–3808.

200 P. Chakraborty, A. Baksi, S. K. Mudedla, A. Nag, G. Paramasivam, V. Subramanian and T. Pradeep, *Phys. Chem. Chem. Phys.*, 2018, 20, 7593–7603.

201 A. Baksi, A. Ghosh, S. K. Mudedla, P. Chakraborty, S. Bhat, B. Mondal, K. R. Krishnadas, V. Subramanian and T. Pradeep, *J. Phys. Chem. C*, 2017, 121, 13421–13427.

202 A. Soleilhac, F. Bertorelle, C. Comby-Zerbino, F. Chirot, N. Calin, P. Dugourd and R. Antoine, *J. Phys. Chem. C*, 2017, 121, 27733–27740.

203 S. Daly, C. M. Choi, A. Zavras, M. Krstic, F. Chirot, T. U. Connell, S. J. Williams, P. S. Donnelly, R. Antoine, A. Giuliani, V. Bonacic-Koutecky, P. Dugourd and R. A. J. O'Hair, *J. Phys. Chem. C*, 2017, 121, 10719–10727.

204 C. Comby-Zerbino, F. Bertorelle, F. Chirot, P. Dugourd and R. Antoine, *Eur. Phys. J. D*, 2018, 72.

205 C. Comby-Zerbino, M. Perić, F. Bertorelle, F. Chirot, P. Dugourd, V. Bonačić-Koutecký and R. Antoine, *Nanomaterials*, 2019, 9, 457.

206 M. R. Ligare, E. S. Baker, J. Laskin and G. E. Johnson, *Chem. Commun.*, 2017, 53, 7389–7392.

207 K. Hirata, P. Chakraborty, A. Nag, S. Takano, K. Koyasu, T. Pradeep and T. Tsukuda, *J. Phys. Chem. C*, 2018, 122, 23123–23128.

208 E. Kalenius, S. Malola, M. F. Matus, R. Kazan, T. Bürgi and H. Häkkinen, *J. Am. Chem. Soc.*, 2021, 143, 1273–1277.

209 C. M. Choi, A. Kulesza, S. Daly, L. MacAleese, R. Antoine, P. Dugourd and F. Chirot, *Rapid Commun. Mass Spectrom.*, 2019, 33, 28–34.

210 A.-L. Simon, F. Chirot, C. M. Choi, C. Clavier, M. Barbaire, J. Maurelli, X. Dagany, L. MacAleese and P. Dugourd, *Rev. Sci. Instrum.*, 2015, 86, 094101.

211 S. Poyer, C. M. Choi, C. Deo, N. Bogliotti, J. Xie, P. Dugourd, F. Chirot and J.-Y. Salpin, *Analyst*, 2020, 145, 4012–4020.

212 R. Hamouda, B. Bellina, F. Bertorelle, I. Compagnon, R. Antoine, M. Broyer, D. Rayane and P. Dugourd, *J. Phys. Chem. Lett.*, 2010, 1, 3189–3194.

213 R. Tomihara, K. Hirata, H. Yamamoto, S. Takano, K. Koyasu and T. Tsukuda, *ACS Omega*, 2018, 3, 6237–6242.

214 A. Zavras, G. N. Khairallah and R. A. J. O'Hair, in *Gold Clusters, Colloids and Nanoparticles II*, ed. D. M. P. Mingos, Springer, New York, 2014, vol. 162, pp. 139–230.

215 D. M. Black, N. Bhattarai, R. L. Whetten and S. B. H. Bach, *J. Phys. Chem. A*, 2014, 118, 10679–10687.

216 F. Bertorelle, I. Russier-Antoine, C. Comby-Zerbino, F. Chirot, P. Dugourd, P. F. Brevet and R. Antoine, *ACS Omega*, 2018, 3, 15635–15642.

217 G. E. Johnson, T. Priest and J. Laskin, *Chem. Sci.*, 2014, 5, 3275–3286.

218 D. M. Black, C. M. Crittenden, J. S. Brodbelt and R. L. Whetten, *J. Phys. Chem. Lett.*, 2017, 8, 1283–1289.

219 M. Jash, R. R. J. Methikkalam, M. Bodiuzzaman, G. Paramasivam and T. Pradeep, *Chem. Commun.*, 2020, 56, 15623–15626.

220 T. Tabarin, R. Antoine, M. Broyer and P. Dugourd, *Eur. Phys. J. D*, 2006, **37**, 237–239.

221 R. Antoine and P. Dugourd, *Phys. Chem. Chem. Phys.*, 2011, **13**, 16494–16509.

222 R. Antoine, J. Lemoine and P. Dugourd, *Mass Spectrom. Rev.*, 2014, **33**, 501–522.

223 A. Cirri, H. M. Hernández and C. J. Johnson, *J. Phys. Chem. A*, 2020, **124**, 1467–1479.

224 A. Cirri, H. Morales Hernández, C. Kmiotek and C. J. Johnson, *Angew. Chem., Int. Ed.*, 2019, **58**, 13818–13822.

225 K. Koyasu and T. Tsukuda, *J. Chem. Phys.*, 2021, **154**, 140901.

226 K. Hirata, R. Tomihara, K. Kim, K. Koyasu and T. Tsukuda, *Phys. Chem. Chem. Phys.*, 2019, **21**, 17463–17474.

227 Ž. Sanader, R. Mitrić, V. Bonačić-Koutecký, B. Bellina, R. Antoine and P. Dugourd, *Phys. Chem. Chem. Phys.*, 2014, **16**, 1257–1261.

228 B. Bellina, I. Compagnon, L. MacAleese, F. Chirot, J. Lemoine, P. Maître, M. Broyer, R. Antoine, A. Kulesza, R. Mitrić, V. Bonačić-Koutecký and P. Dugourd, *Phys. Chem. Chem. Phys.*, 2012, **14**, 11433–11440.

229 R. Antoine, T. Tabarin, M. Broyer, P. Dugourd, R. Mitric and V. Bonacic-Koutecky, *ChemPhysChem*, 2006, **7**, 524–528.

230 I. Compagnon, T. Tabarin, R. Antoine, M. Broyer, P. Dugourd, R. Mitric, J. Petersen and V. Bonacic-Koutecky, *J. Chem. Phys.*, 2006, **125**, 164326.

231 R. Antoine, F. Bertorelle, M. Broyer, I. Compagnon, P. Dugourd, A. Kulesza, R. Mitric and V. Bonacic-Koutecky, *Angew. Chem., Int. Ed.*, 2009, **48**, 7829–7832.

232 A. Kulesza, R. Mitric, V. Bonacic-Koutecky, B. Bellina, I. Compagnon, M. Broyer, R. Antoine and P. Dugourd, *Angew. Chem., Int. Ed.*, 2011, **50**, 878–881.

233 B. Bellina, R. Antoine, M. Broyer, L. Gell, Z. Sanader, R. Mitric, V. Bonacic-Koutecky and P. Dugourd, *Dalton Trans.*, 2013, **42**, 8328–8333.

234 T. Tabarin, A. Kulesza, R. Antoine, R. Mitric, M. Broyer, P. Dugourd and V. Bonacic-Koutecky, *Phys. Rev. Lett.*, 2008, **101**, 213001.

235 Y. T. Yang, C. Callegari, X. L. Feng, K. L. Ekinci and M. L. Roukes, *Nano Lett.*, 2006, **6**, 583–586.

236 S. Dominguez-Medina, S. Fostner, M. Defoort, M. Sansa, A.-K. Stark, M. A. Halim, E. Vernhes, M. Gely, G. Jourdan, T. Alava, P. Boulanger, C. Masselon and S. Hentz, *Science*, 2018, **362**, 918–922.

237 H. Fakhouri, M. Perić, F. Bertorelle, P. Dugourd, X. Dagany, I. Russier-Antoine, P.-F. Brevet, V. Bonačić-Koutecký and R. Antoine, *Phys. Chem. Chem. Phys.*, 2019, **21**, 12091–12099.

238 G. F. Combes, H. Fakhouri, C. Moulin, M. Girod, F. Bertorelle, S. Basu, R. Ladouce, M. Perić Bakulić, Ž. Sanader Maršić, I. Russier-Antoine, P.-F. Brevet, P. Dugourd, A. Krisko, K. Trajković, M. Radman, V. Bonačić-Koutecký and R. Antoine, *Commun. Chem.*, 2021, **4**, 69.

239 I. Russier-Antoine, F. Bertorelle, A. Kulesza, A. Soleilhac, A. Bensalah-Ledoux, S. Guy, P. Dugourd, P. F. Brevet and R. Antoine, *Prog. Nat. Sci.: Mater. Int.*, 2016, **26**, 455–460.

240 O. V. Lushchikova, D. M. M. Huitema, P. López-Tarifa, L. Visscher, Z. Jamshidi and J. M. Bakker, *J. Phys. Chem. Lett.*, 2019, **10**, 2151–2155.

241 A. Fielicke, C. Ratsch, G. V. Helden and G. Meijer, *J. Chem. Phys.*, 2005, **122**, 091105.

242 K. Hirata, K. Yamashita, S. Muramatsu, S. Takano, K. Ohshimo, T. Azuma, R. Nakanishi, T. Nagata, S. Yamazoe, K. Koyasu and T. Tsukuda, *Nanoscale*, 2017, **9**, 13409–13412.

243 S. Daly, F. Rosu and V. Gabelica, *Science*, 2020, **368**, 1465–1468.

244 R. Hadidi, D. K. Bozanic, G. A. Garcia and L. Nahon, *Adv. Phys.: X*, 2018, **3**, 1477530.

245 E. R. Gran, F. Bertorelle, H. Fakhouri, R. Antoine, M. Perić Bakulić, Ž. Sanader Maršić, V. Bonačić-Koutecký, M. Blain, J. Antel and D. Maysinger, *Nanoscale*, 2021, **13**, 3173–3183.

246 J. Ji, A. Moquin, F. Bertorelle, P. Ky Chang, R. Antoine, J. Luo, R. A. McKinney and D. Maysinger, *Nanotoxicology*, 2019, **13**, 285–304.

247 D. Maysinger, E. R. Gran, F. Bertorelle, H. Fakhouri, R. Antoine, E. S. Kaul, D. M. Samhadaneh and U. Stochaj, *Theranostics*, 2020, **10**, 1633–1648.

248 E. C. Dreaden, A. M. Alkilany, X. Huang, C. J. Murphy and M. A. El-Sayed, *Chem. Soc. Rev.*, 2012, **41**, 2740–2779.

249 P. Y. B. Florian, M. A. H. Ron and P. Nina Ogrinc, *Curr. Pharm. Des.*, 2017, **23**, 1974–1984.

250 S. Bose, A. Chatterjee, S. K. Jenifer, B. Mondal, P. Srikrishnarka, D. Ghosh, A. R. Chowdhuri, M. P. Kannan, S. V. Elchuri and T. Pradeep, *ACS Sustainable Chem. Eng.*, 2021, **9**, 4554–4563.

251 A. Pawar, S. Thakkar and M. Misra, *J. Controlled Release*, 2018, **286**, 179–200.

252 J. A. Tapia-Hernández, P. I. Torres-Chávez, B. Ramírez-Wong, A. Rascón-Chu, M. Plascencia-Jatomea, C. G. Barreras-Urbina, N. A. Rangel-Vázquez and F. Rodríguez-Félix, *J. Agric. Food Chem.*, 2015, **63**, 4699–4707.

253 C. Luo, T. Okubo, M. Nangrejo and M. Edirisinghe, *Polym. Int.*, 2015, **64**, 183–187.

254 M. Vojkovic, D. Rayane, R. Antoine, M. Broyer, A. R. Allouche, P. Mignon and P. Dugourd, *J. Phys. Chem. A*, 2017, **121**, 4404–4411.

255 M. Vojkovic, D. Rayane, F. Bertorelle, R. Antoine, M. Broyer and P. Dugourd, *Int. J. Mass Spectrom.*, 2015, **387**, 45–50.

256 M. P. Woodard, S. T. Akin, C. J. Dibble and M. A. Duncan, *J. Phys. Chem. A*, 2018, **122**, 3606–3620.

257 M. Perić, Ž. Sanader Maršić, I. Russier-Antoine, H. Fakhouri, F. Bertorelle, P.-F. Brevet, X. le Guével, R. Antoine and V. Bonačić-Koutecký, *Phys. Chem. Chem. Phys.*, 2019, **21**, 23916–23921.